A.R.A.P. REPORT NO. 203 NASA CR-132369

A PRELIMINARY SENSITIVITY ANALYSIS OF THE COUPLED DIFFUSION AND CHEMISTRY MODEL

Glenn R. Hilst
Ross M. Contiliano

Prepared under Contract NAS1-12475 by
Aeronautical Research Associates of Princeton, Inc.
50 Washington Road, Princeton, New Jersey 08540

for

NATIONAL AERONAUTICS AND SPACE ADMINISTRATION

October 1973

ABSTRACT

The sensitivity of the coupled chemistry/diffusion model's outputs to a wide range of variation of the model's independent variables has been investigated. It is shown that the efficiency with which the NO_x catalytic cycle destroys ambient O_3 is extremely sensitive to the amount of NO emitted and to the relative rates of turbulent diffusion and chemical reactions. For representative conditions in the stratosphere, a tenfold variation of either the turbulence intensity or the reaction rate constant or the source strength can vary the efficiency from 1% to 50%. If the duration of Phase III is a significant fraction of the total residence time of the plume, then these efficiency variations can alter O_3 depletion rates by more than a factor of two. These results, therefore, point toward those variables which must be accurately defined or measured if one is to adequately predict the effect of SST operations on the ambient inventory of O_3 in the lower stratosphere.

A PRELIMINARY SENSITIVITY ANALYSIS OF THE COUPLED DIFFUSION AND CHEMISTRY MODEL

Glenn R. Hilst

Ross M. Contiliano

Aeronautical Research Associates of Princeton, Inc.

INTRODUCTION

Since the summer of 1972, A.R.A.P. has developed a second-order closure scheme for isothermal reactions in a binary chemical system. This chemical kinetics model has been successfully coupled with the invariant turbulence and diffusion models for the case of two-dimensional diffusion of two reacting chemical species which emanate from common or separate sources. The coupled model, while still necessarily an approximation, retains the second-order correlations for both species concentrations and turbulent motions and therefore permits separate evaluation of the flux divergences and inhomogeneous chemical reaction rates in the mass conservation equations for the reacting species. References 1 and 2 describe the development of this coupled model and the results of some preliminary applications to the SST exhaust plume. We will try to avoid repetitions of those discussions in this report.

The coupled model represents a substantial improvement in the simulation of chemical reactions in turbulent flow fields. Conventional techniques may fail to adequately describe the fate of SST exhaust products because of two severe limitations. First, because these techniques employ first-order closure and assume that the local reaction rate proceeds according to the local mean value of the species concentrations, they fail to account for spatial inhomogeneities of the two reactants and the possible reduction of the

reaction rate due to the correlated concentration fluctuations ($\overline{C'_\alpha C'_\beta}$). In contrast, second-order closure permits dynamic simulation of this "mixedness" term and thereby permits quantitative evaluation of the effects of spatial inhomogeneity. Some of the work reported here demonstrates a mixedness limitation approaching 25% for equilibrium conditions and even larger effects for non-equilibrium conditions and in the core of the plume. Whether such an effect is significant depends on the uncertainty one wishes to attach to each of the independent variables of the model.

A second and more serious limitation of conventional techniques for stratospheric plumes is the decoupling of the chemical depletion and turbulent diffusion processes and the assumption that the reactants are always intimately mixed. This assumption completely ignores the experimental evidence that the stratosphere is stably stratified and, for the most part, is in nearly laminar motion. It is quite possible that due to very slow turbulent diffusion the ambient species may be rapidly depleted by chemical reaction in the center of the plume and only slowly replenished by diffusion. As a result, significant portions of the plume may be shielded from the environmental species (as long as plume concentrations remain high) and such plumes may survive considerably longer than previously estimated.

The second-order closure model may be utilized in situations ranging from those in which vigorous mixing and slow chemistry make the flux divergence completely dominant, to situations of slow diffusion and fast chemical reactions in which the reaction rate dominates. Preliminary results, simulating the reaction of O_3 with NO in the post-vortex SST exhaust plume have demonstrated a strong diffusion limitation on this reaction in the stratosphere - a condition which may persist for days to weeks.

The work reported upon here is an extension of these early results in the form of a sensitivity analysis of the model's response to systematic variations of the input variables. In addition to the determination of the sensitivity of the model outputs to the input parameters, and therefore knowledge of how well these input parameters must be known for reliable results, the choices of the ranges and values of each input parameter based on realistic values provides a first "catalog" of the expected ranges and interactions of diffusive and chemical processes in the SST far wake. These results may both guide and be verified by the NASA stratospheric jet wake experiments. They will also provide guidelines as to when conventional decoupled chemistry and diffusion models may be used and when coupled models are required for useful estimates of the far wake behavior. Finally, these results will be extremely useful in structuring three-dimensional models.

SYMBOLS

a_i	constant evaluated using Eq. (18)
C_i	concentration of ith chemical species
E	chemical efficiency defined by Eq. (33)
$\overline{E}$	average efficiency for residence time of plume
f_i	transfer function
k	reaction rate constant
K	constant in Eq. (6)
L_D	diffusion limitation defined by Eq. (34)
L_M	mixedness limitation defined by Eq. (35)
P	any dependent variable
q	twice the square root of the turbulent kinetic energy
Q	amount of NO emitted per unit distance of travel and per unit width of plume
R	total reaction rate in plume defined by Eq. (31)
R^*	maximum reaction rate in plume
Ri	Richardson number
Ri_c	critical Richardson number
S_α	source or sink of α chemical species
S_i	slope of iso-x_{i+1} contour in nomogram
t	time
t_d	time required to dilute plume by 10^3
$\overline{T}$	potential temperature
T_R	residence time of plume
u	longitudinal velocity
v	lateral velocity

w	vertical velocity
x	longitudinal distance
y	lateral distance
z	vertical distance
ϵ_o	Arrhenius activation energy
κ	Boltzmann constant
Λ_D	diffusive scale length
Λ_T	turbulence scale length
ν	kinematic viscosity of fluid
σ	standard deviation

superscripts

$\overline{}$	mean component
'	fluctuating component

subscripts

chem	depletion rate due to chemical reactions
e	environmental value
α	O_3 chemical species
β	NO chemical species
γ, δ	reactive chemical species other than O_3 or NO
M	unreactive chemical species

THE COUPLED DIFFUSION/CHEMISTRY MODEL

The coupled model was developed for the following conditions:

1. Incompressible flow
2. Binary and isothermal chemical reactions
3. Horizontally homogeneous turbulence

4. No coupling between the chemical reactions and the turbulence field.
5. Horizontal straight-line flow with the mean wind speed, $\overline{U}$, a function of height only.
6. Two-dimensional (z and t) coupled diffusion and chemistry (i.e. lateral and longitudinal diffusion negligible in comparison with the vertical component).

Despite these apparent restrictions, the model does capture a large part of the SST wake features and does permit the first critical study of the interaction between diffusion and chemistry in a turbulent, inhomogeneous system. In the future, each of these constraints will be removed, although the additional computational complexity will be considerable. It therefore behooves us to exercise the present model vigorously in order to pave the way for this future work.

We consider the irreversible binary chemical reaction between chemical species α and β to form γ and δ.

$$\alpha + \beta \rightarrow \gamma + \delta \tag{1}$$

The constituents satisfy the species conservation equation

$$C_\alpha + C_\beta + C_\gamma + C_\delta + C_M = 1 \tag{2}$$

where C_i is the concentration of the ith chemical species and M represents all nonreactants in the reaction volume. We assume that the reaction rate for any joint value of the concentrations is given by

$$\left[\frac{\partial C_\alpha}{\partial t}\right]_{chem} = - k_1 C_\alpha C_\beta \tag{3}$$

$$\left[\frac{\partial C_\beta}{\partial t}\right]_{chem} = - k_2 C_\alpha C_\beta \tag{4}$$

and that

$$\frac{\partial}{\partial t}\left[C_\gamma + C_\delta\right] = - \frac{\partial}{\partial t}\left[C_\alpha + C_\beta\right] \tag{5}$$

where k_i are the reaction rate constants and are given by the Arrhenius equation

$$k_i = KT^M \exp\left(\epsilon_o/\kappa T\right) \tag{6}$$

Equations (3) and (4) represent the local instantaneous rate of change of the concentration due to chemical reaction. In order to determine the average rate of change, we assume the history of the joint values of C_α and C_β at a fixed location comprises a stationary time series and each may be dissected into its mean and fluctuating components

$$C_i = \overline{C}_i + C_i' \tag{7}$$

and, by definition, $\overline{C}_i' = 0$. Under these assumptions, the equations for the average rates of change of α and β become

$$\left[\frac{\partial \overline{C}_\alpha}{\partial t}\right]_{chem} = -k_1(\overline{C}_\alpha \overline{C}_\beta + \overline{C_\alpha' C_\beta'}) \tag{8}$$

$$\left[\frac{\partial \overline{C}_\beta}{\partial t}\right]_{chem} = -k_2(\overline{C}_\alpha \overline{C}_\beta + \overline{C_\alpha' C_\beta'}) \tag{9}$$

and similarly the species conservation Eq. (2) becomes

$$\overline{C}_\alpha + \overline{C}_\beta + \overline{C}_\gamma + \overline{C}_\delta + \overline{C}_M = 1 \tag{10}$$

$$C_\alpha' + C_\beta' + C_\gamma' + C_\delta' + C_M' = 0 \tag{11}$$

Now, the equation for the conservation of mass of the α species may be written

$$\frac{DC_\alpha}{Dt} = \frac{\partial C_\alpha}{\partial t} + u\frac{\partial C_\alpha}{\partial x} + v\frac{\partial C_\alpha}{\partial y} + w\frac{\partial C_\alpha}{\partial t}$$

$$= \nu\left(\frac{\partial^2 C_\alpha}{\partial x^2} + \frac{\partial^2 C_\alpha}{\partial y^2} + \frac{\partial^2 C_\alpha}{\partial z^2}\right) + \left[\frac{\partial C_\alpha}{\partial t}\right]_{chem} + S_\alpha \tag{12}$$

and a similar equation may be written for the β species. In Eq. (12) u, v, w are the instantaneous velocity components in the x, y, z directions, respectively, ν is the fluid kinematic viscosity, and S_α includes all sources and sinks not directly attributable to chemical alteration according to Eqs. (3) and (4).

If we assume that an ensemble average of the physical variables in the frame of reference is statistically stationary we can write any of the variables in terms of its mean and fluctuating components. If we do this in Eq. (12) and then time average the resulting equation according to Reynolds rules, we obtain

$$\frac{\partial \overline{C}_\alpha}{\partial t} + \overline{u}\frac{\partial \overline{C}_\alpha}{\partial x} + \overline{v}\frac{\partial \overline{C}_\alpha}{\partial y} + \overline{w}\frac{\partial \overline{C}_\alpha}{\partial z} = \nu\left(\frac{\partial^2 \overline{C}_\alpha}{\partial x^2} + \frac{\partial^2 \overline{C}_\alpha}{\partial y^2} + \frac{\partial^2 \overline{C}_\alpha}{\partial z^2}\right)$$

$$- \frac{\partial}{\partial x}\overline{C'_\alpha u'} - \frac{\partial}{\partial y}\overline{C'_\alpha v'} - \frac{\partial}{\partial z}\overline{C'_\alpha w'} - k_1(\overline{C}_\alpha \overline{C}_\beta + \overline{C'_\alpha C'_\beta}) + S_\alpha \quad (13)$$

and similarly for $\overline{C}_\beta$.

For convenience we assume a statistically steady state (i.e. $\partial/\partial t = 0$) , a coordinate system aligned with the flow direction (i.e. $\overline{v} = \overline{w} = 0$ and $\overline{u} = \overline{u}(z)$) , invoke the two-dimensional ($\partial/\partial y = 0$) and boundary layer assumptions ($\partial/\partial x << \partial/\partial z$) and consider no sources or sinks of α (or β) downstream of a continuous line source of either species. We then obtain the following final form of the mass balance equations.

$$\overline{u}\frac{\partial \overline{C}_\alpha}{\partial x} = \nu\frac{\partial^2 \overline{C}_\alpha}{\partial z^2} - \frac{\partial}{\partial z}\overline{C'_\alpha w'} - k_1(\overline{C}_\alpha \overline{C}_\beta + \overline{C'_\alpha C'_\beta}) \quad (14)$$

$$\overline{u}\frac{\partial \overline{C}_\beta}{\partial x} = \nu\frac{\partial^2 \overline{C}_\beta}{\partial z^2} - \frac{\partial}{\partial z}\overline{C'_\beta w'} - k_2(\overline{C}_\alpha \overline{C}_\beta + \overline{C'_\alpha C'_\beta}) \quad (15)$$

In order to solve Eqs. (14) and (15), we require seven additional partial differential equations for $\overline{C'_\alpha w'}$, $\overline{C'_\beta w'}$, $\overline{C'^2_\alpha}$, $\overline{C'^2_\beta}$, $\overline{C'_\alpha C'_\beta}$, $\overline{C'_\alpha T'}$, $\overline{C'_\beta T'}$ and three additional algebraic equations for the third-order moments $\overline{C'^2_\alpha C'_\beta}$, $\overline{C'_\alpha C'^2_\beta}$, $\overline{C'_\alpha C'_\beta T}$. These equations are derived in both refs. 1 and 2 for the interested reader.

In this analysis we have focused on the critical problem of the destruction of O_3 by the NO_x catalytic cycle. Our simulation of the NO_x catalytic cycle is a simplified one which treats only the simultaneous diffusive mixing and reaction of O_3 with NO under the assumption of the immediate restoration (and therefore conservation) of NO by the reaction of NO_2 with O. The NO_x catalytic cycle

$$NO + O_3 \rightarrow NO_2 + O_2 \quad (16)$$

$$NO_2 + O \rightarrow NO + O_2 \quad (17)$$

can be approximated for model solution by assuming that NO + NO_2 = NO_x is conserved and the ratio of NO to NO_2 is a constant in time. This implies the further assumption that the restoration of NO by Eq. (17) is not limited by the supply of O; a questionable assumption in the dark sky since O is produced primarily by photolysis of O_3 and NO_2. This system cannot pretend to follow all of the factors which contribute to the quasi-equilibrium concentrations in the lower stratosphere. However, the combined diffusion and simplified chemical reaction model used here does capture the main features of the NO_x catalytic cycle in controlling the local fate of O_3 during most turbulent diffusion regimes to be expected in the lower stratosphere. The most questionable assumption is that the production of O_3 in the plume is negligible.

DESCRIPTION OF COMPUTATION MATRIX

A total of 213 computations were made using various combinations of the input variables to the coupled chemistry/diffusion model in order to simulate the reaction of O_3 with NO in the post-vortex SST plume. These computations required approximately 500 hours on the META-4 computer system. The primary input variables which were investigated were: (1) the turbulence field, (2) the source strength and geometry of the initial species concentrations, and (3) the reaction rate constants. In addition, 20 computations were made using the three dimensional diffusion model to investigate the effect of the diffusion scale length on plume growth. These computations required approximately 100 hours on the META-4.

Table 1 summarizes the range of variation for each of the input variables. The following paragraphs describe this computation matrix.

TABLE 1

RANGE OF INPUT VARIABLES		
Variable		Values
Turbulence Field	Ri	0, .1, .2, .35, .5
	Λ_T	50, 100, 200, 500, 1000 meters
Source Geometry and Strength	σ_z	25, 50, 100 meters
	σ_y	10^2, 10^3, 10^4, 3×10^4, 10^5 meters
Reaction Rate Constant	k_1	5×10^5, 5×10^4, 5×10^3, 5×10^2 $\frac{1}{\text{pp-sec}}$
Diffusion Scale Length	$\frac{\Lambda_D}{\Lambda_T}$	1., 2.5, 5, 10

The Turbulence Field

The turbulence field was simulated by the decoupled invariant turbulence model. The inputs to this model are the mean wind speed and temperature profiles for the altitude interval of interest and three scale lengths which are derived from best estimates of the integral scale length (Λ_T) of the turbulent motions.

The ranges of mean wind shear and temperature lapse rates are fairly well known for the lower stratosphere. For this study, five combinations of shear ($\partial\overline{u}/\partial z$) and potential temperature lapse rate ($\partial\overline{T}/\partial z$) were chosen to simulate varying degrees of stability. The five combinations corresponded to Richardson numbers of 0 (neutrally stable) to 0.5 (highly stable) and are illustrated in Fig. 1. Note that the present model parameters used in the turbulence model yield a critical Richardson number of 0.55. Therefore, all of the flow fields used in this analysis were based on equilibrium turbulence.

Quantitative information regarding the integral scale length of the turbulence in the lower stratosphere is meager. In order to examine the sensitivity of the chemistry/diffusion model to variations in the turbulence field produced by changes in the integral scale length, we have chosen five values of the scale length for each of the five above-mentioned Richardson numbers. Thus, twenty-five ($5\ \Lambda_T \times 5\ \mathrm{Ri}$) different turbulence fields were investigated.

Because for the purposes of this analysis, the wind shear and temperature lapse rates are functions of Richardson number, the equilibrium turbulence field is completely specified by the combination of Ri and Λ_T. In Figs. 2 - 5, we show the sensitivity to Ri and Λ_T of the turbulence parameters which are inputs to the chemistry/diffusion model.

Figures 2 and 3 show the turbulent energy (q^2) and the vertical velocity fluctuations ($\overline{w'^2}$) respectively. In each case, there is a strong dependence on both Ri and Λ_T. Each decreases rapidly as Ri increases and each is directly proportional to Λ_T^2.

Figure 4 shows the Reynolds stress ($\overline{u'w'}$). It rapidly approaches 0 as Ri increases and is directly proportional to Λ_T^2.

Figure 5 shows the vertical heat flux ($\overline{w'T'}$). The sensitivity to Ri is different from the preceding parameters because the heat flux is 0 not only when $\mathrm{Ri} \geq \mathrm{Ri}_c = 0.55$ but also when there is no potential temperature gradient (i.e. Ri = 0). For a given Ri, the heat flux is directly proportional to Λ_T^2.

Table 2 shows the breakdown of the computation matrix for each combination of Ri and Λ_T. The computations were about equally distributed with respect to Ri with 42% of the runs in the highly stable regime ($\mathrm{Ri} \geq .35$) and 49% in the neutral or nearly neutral regime ($\mathrm{Ri} \leq .1$). Approximately 80% of the runs were for scale lengths in the range $100 \leq \Lambda_T \leq 500$ meters.

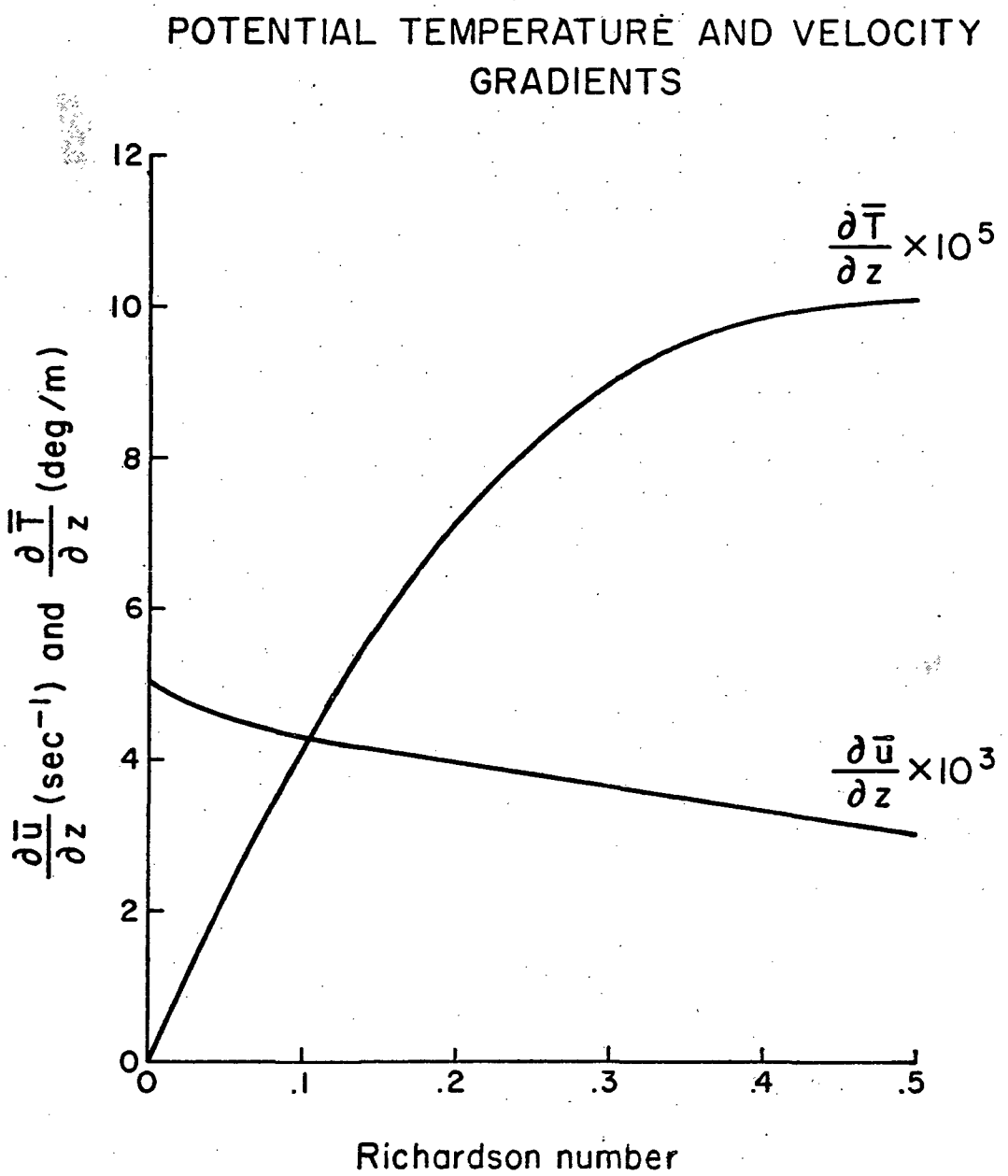

Figure 1. The combinations of wind shear and potential temperature lapse rate which were used to simulate varying degrees of stability in the lower stratosphere.

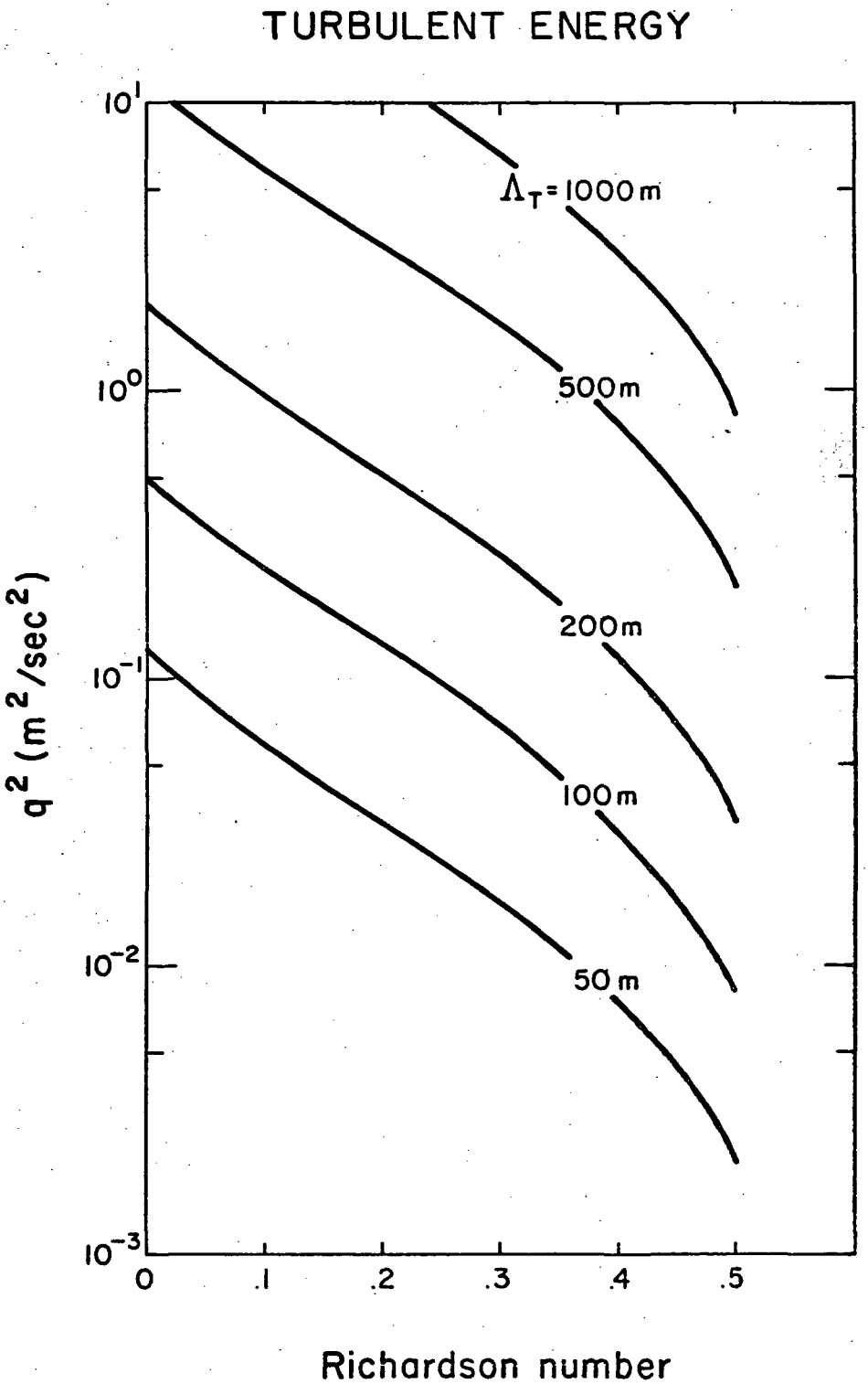

Figure 2. The sensitivity of the turbulent kinetic energy to Richardson number and to the turbulence scale length.

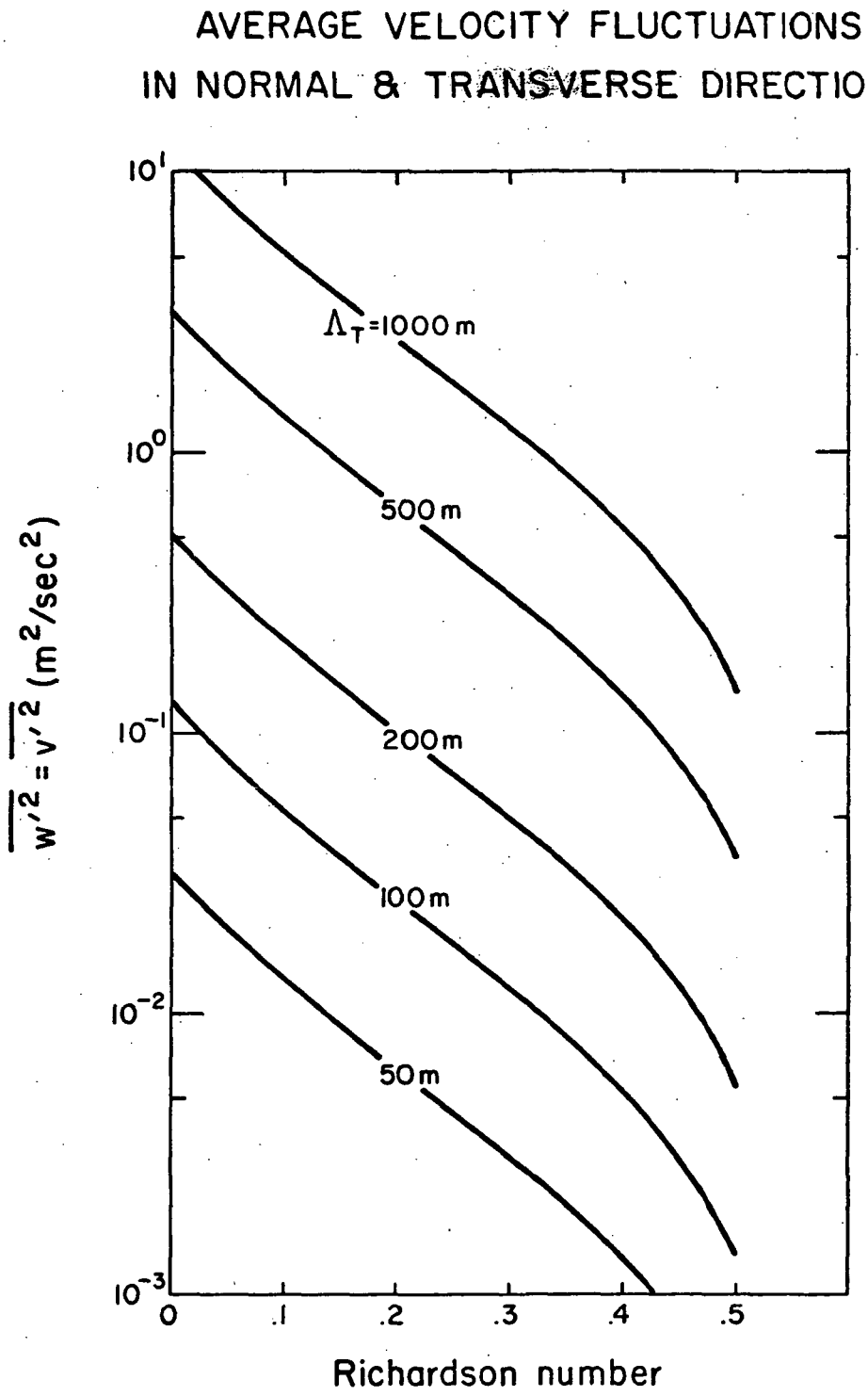

Figure 3. The sensitivity of the average velocity fluctuations in the vertical and lateral directions to Richardson number and to the turbulence scale length.

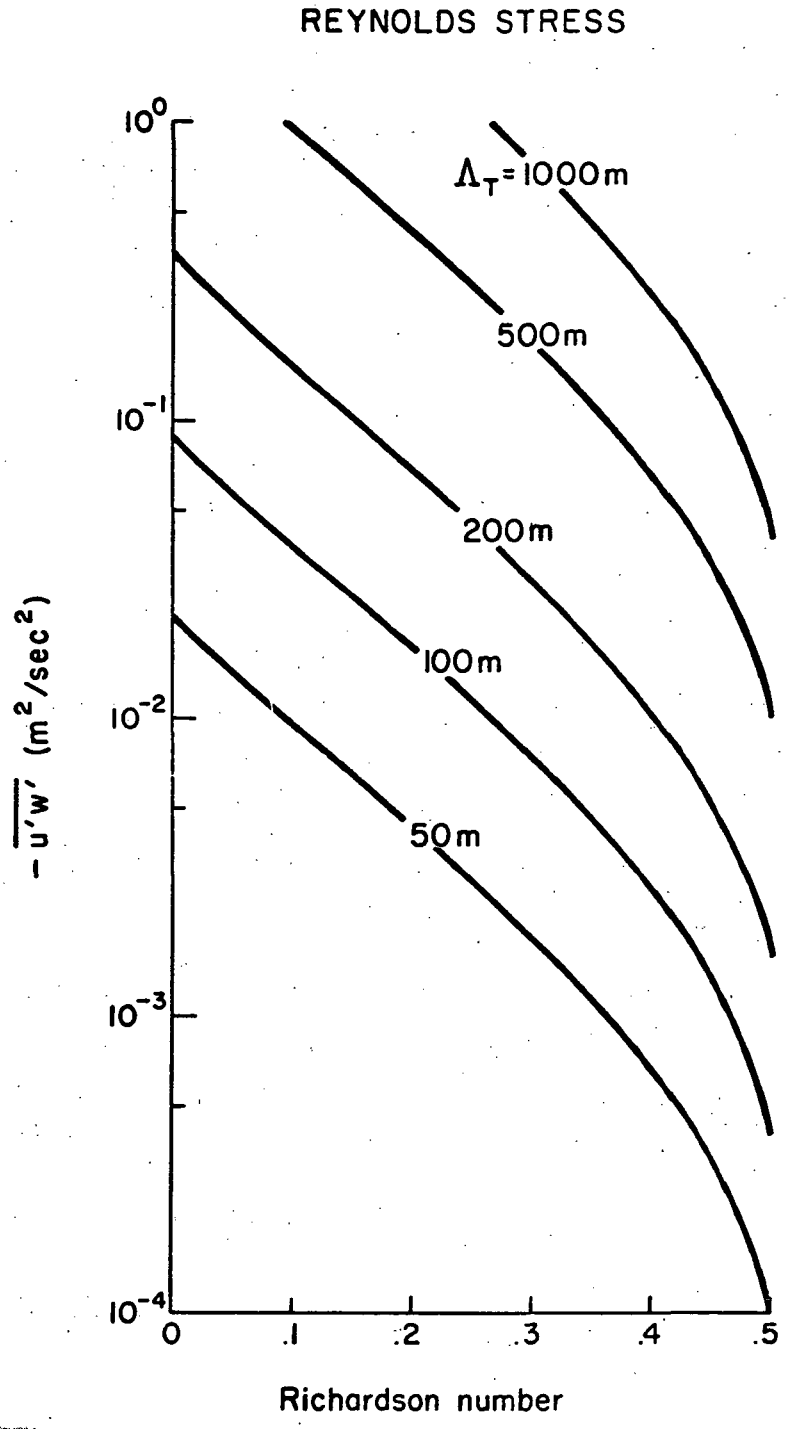

Figure 4. The sensitivity of the average Reynolds stress to Richardson number and to the turbulence scale length.

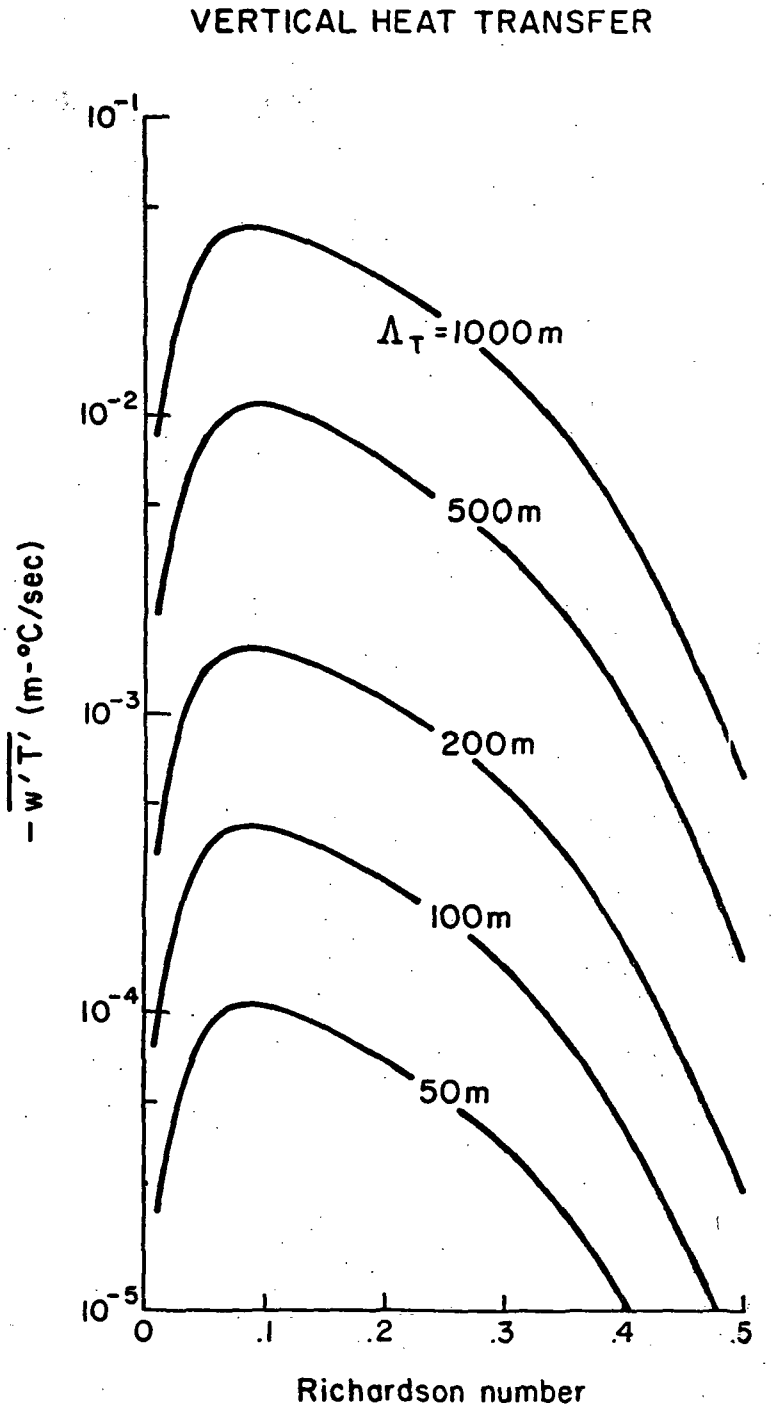

Figure 5. The sensitivity of the average vertical heat flux to Richardson number and to the turbulence scale length.

TABLE 2

BREAKDOWN OF RUNS FOR Ri AND Λ_T						
Richardson Number (Ri)	Turbulence Scale Length (Λ_T)					Totals
	50m	100m	200m	500m	1000m	
0	2	12	2	7	2	25
.1	9	32	13	20	4	78
.2	2	8	2	5	2	19
.35	5	30	4	7	9	55
.5	9	16	2	7	2	36
Totals	27	98	23	46	19	213

Table 3 shows the run breakdown of the turbulence fields in terms of decades in q^2. Note that the analysis was performed for a five decade range of q^2 and that about 40% of the computations were in the interval $10^{-3} \leq q^2 \leq 10^{-1}$ meter^2/sec^2.

TABLE 3

BREAKDOWN OF RUNS FOR q^2	
q^2 Interval (m^2/sec^2)	Number of Runs
10^{-3} - 10^{-2}	25
10^{-2} - 10^{-1}	62
10^{-1} - 10^{0}	68
10^{0} - 10^{1}	43
10^{1} - 10^{2}	15
Total	213

Source Geometry and Strength

We assumed that the initial NO concentration distribution was bivariant normal and therefore could be specified by a central value and horizontal and vertical variances, σ_y^2 and σ_z^2, in the following manner

$$\overline{C}_i(z,y) = \frac{a_i}{\sigma_y \sigma_z} \exp\left[-\frac{1}{2}\left(\frac{y^2}{\sigma_y^2} + \frac{z^2}{\sigma_z^2}\right)\right] \qquad (18)$$

where a_i is a constant to be evaluated from the initial source strength for NO. For the purposes of this analysis, as an initial condition the NO was symmetrically distributed about the axis of the plume with a standard deviation of 25 meters in both directions (i.e. $\sigma_y = \sigma_z = 25$ m) and a centerline concentration of 2×10^{-6}ppp. The O_3 was assumed to be initially distributed in a complementary gaussian profile with an ambient value, outside the plume, of 2×10^{-6}ppp. For these conditions, $a_i = 1.25\times10^{-3}$ppp m^2.

The present coupled model considers diffusion in the vertical direction only. The initial concentration profile is given by

$$\overline{C}(z) = \overline{C}_i(0,0) \exp\left[-\frac{1}{2}\frac{z^2}{\sigma_z^2}\right] \qquad (19)$$

and $\overline{C}_i(0,0)$ is obtained from Eq. (18) for each combination of σ_y and σ_z. Table 4 summarizes the values of the initial centerline concentrations for each of the source geometries.

TABLE 4

INITIAL CENTERLINE CONCENTRATION (ppp)					
σ_z (meters)	σ_y (meters)				
	10^2	10^3	10^4	3×10^4	10^5
25	$.5\times10^{-6}$	$.5\times10^{-7}$	$.5\times10^{-8}$	$.15\times10^{-8}$	$.5\times10^{-9}$
50	$.25\times10^{-6}$	$.25\times10^{-7}$	$.25\times10^{-8}$	$.75\times10^{-9}$	$.25\times10^{-9}$
100	$.125\times10^{-6}$	$.125\times10^{-8}$	$.375\times10^{-9}$	$.375\times10^{-9}$	$.125\times10^{-9}$

Thus, a combination of σ_y and σ_z may be related to a particular time in the diffusion of a plume whose source strength is fixed.

Alternatively, because only σ_z enters the coupled model directly, σ_y may be used as a measure of the source strength as follows. Consider the total amount (Q) of NO in a vertical column per unit distance of travel and per unit width of the plume.

$$Q = \int_{-\infty}^{\infty} \overline{C}(z)\, dz \tag{20}$$

If we integrate Eq. (20) using Eq. (19), then

$$Q = \sqrt{2\pi}\ \sigma_z\ \overline{C}_i(0,0) \tag{21}$$

But, by Eq. (18)

$$\overline{C}_i(0,0) = \frac{a_i}{\sigma_y \sigma_z} \tag{22}$$

and, therefore,

$$Q = \frac{\sqrt{2\pi a_i}}{\sigma_y} \tag{23}$$

Because a_i is constant, Eq. (23) demonstrates that the amount of NO in a vertical column (i.e. the source strength) is inversely proportional to σ_y. Thus, if we compare computations at a fixed time after emission, then σ_y determines the source strength and σ_z determines the distribution of NO for a fixed strength.

In Table 5, we summarize the number of runs used for each combination of σ_y and σ_z. Approximately one half of the runs were for $\sigma_y = 10^2$ meters. Less than 5% of the runs were for $\sigma_y > 10^4$ meters.

TABLE 5

BREAKDOWN OF RUNS FOR σ_y and σ_z

Vertical Spread σ_z (meters)	Horizontal Spread ~ σ_y (meters)					Total
	10^2	10^3	10^4	3×10^4	10^5	
25	55	12	21	0	0	88
50	28	14	17	4	6	69
100	31	6	19	0	0	56
Total	114	32	57	4	6	213

Approximately 40% of the runs were for $\sigma_z = 25$ m and the remainder of the runs were about evenly divided between $\sigma_z = 50$ m and $\sigma_z = 100$ m .

Reaction Rate Constant

We have chosen a simplified version of the NO_x catalytic cycle for the destruction of O_3. We have assumed that the rate of production of O_3 in the exhaust plume during the early post-vortex stage is negligibly small compared to the destruction of O_3 by NO and that photolysis of NO_2 and the abundance of O in the plume are sufficient to restore all NO_2 to $NO + O_2$. Thus, the catalytic cycle is simply

$$NO + O_3 \rightarrow NO_2 + O_2 \tag{24}$$

$$NO_2 + O \rightarrow NO + O_2 \tag{25}$$

and

$$\left[\frac{\partial}{\partial t}[\overline{O}_3]\right]_{chem} = -k_1\left[[\overline{O}_3][\overline{NO}] + \overline{[O_3]'[NO]'}\right] \tag{26}$$

$$\left[\frac{\partial}{\partial t}[\overline{NO}]\right]_{chem} = 0 \tag{27}$$

The sensitivity of the model to k_1 was investigated by varying k_1 through four orders-of-magnitude from 5×10^5 to 5×10^2 $(pp - sec)^{-1}$. Table 6 summarizes the number of runs for each k_1 .

TABLE 6

BREAKDOWN OF RUNS FOR k_1	
k_1 ($\frac{1}{pp\text{-}sec}$)	Number of Runs
5×10^5	122
5×10^4	31
5×10^3	31
5×10^2	29
Total	213

About 60% of the runs were with $k_1 = 5 \times 10^5$ l/pp-sec. and the balance of the runs were equally distributed among the other three values of k_1 .

Diffusion Scale Length

Extensive experimentation has shown that during the initial phase of plume diffusion the diffusion scale length is correctly determined by the width of the diffusing plume. At some point, however, this scale length becomes constant and the diffusion process goes over to the classical Fickian rate. It can be shown that the upper limiting value of the scale length (Λ_D) is proportional to the turbulence scale (Λ_T) although the constant of proportionality is poorly defined. We have examined four ratios of Λ_D/Λ_T (1, 2.5, 5 and 10) for each of five turbulence fields.

Since the NO is conserved by the NO_x catalytic cycle, the diffusion of NO can be decoupled from the chemistry. Therefore, the sensitivity of the plume growth to changes in Λ_D/Λ_T could be investigated using our three-dimensional diffusion model. The results of these 20 computations together with the results of the 213 computations using the coupled chemistry/diffusion model are discussed in the following sections.

DISCUSSION OF SENSITIVITY ANALYSIS

In this section, we present the results of a sensitivity analysis of the two-dimensional coupled chemistry/diffusion model (as well as the three-dimensional diffusion model) to the primary independent variables of the model. We will concentrate on the principal output parameters of the models such as plume growth, total reaction rates, etc. Keep in mind, however, that by emphasizing these results, we will, of necessity, omit a wealth of data relating to the details of the computations. For example, the time histories of the profiles of all turbulent correlations and the various balances which exist between the fluxes of these correlations in the dynamic equations are available but are not shown. These details can be described at a later date when more detailed measurements of jet wakes become available.

Plume Growth

In our model of the NO_x catalytic cycle, the NO is conserved and therefore acts as a surrogate tracer for any nonreactive exhaust product. Hence, we can separate the effects of turbulent diffusion and chemistry by following the growth of the NO plume. To do this, we have calculated the three-dimensional diffusion history of a plume, for which the initial horizontal and vertical variances are 625 m^2, over a time interval corresponding to a concentration

dilution of nearly 10^4. These calculations were made for five equilibrium turbulence fields for which the intensity of turbulence, q^2, varied from 0.008 to 0.5 m^2/sec^2, Ri from 0 to 0.5, and the scale length of the turbulence, Λ_T, was 100 meters.

The independent variables of the diffusion model are the mean wind shear and potential temperature lapse rates (which together define Ri), the intensity of turbulence, the vertical and lateral velocity fluctuations, and the vertical heat transfer. The sensitivity of each of these variables to Ri and to Λ_T was previously described in Figs. 1-3 and 5.

Besides these inputs, the diffusion model requires specification of the diffusive scale length, Λ_D. This latter length is analogous to, but not necessarily the same as, the turbulence scale length because Λ_D depends on the dimensions of the plume. Prior applications of this model have shown that the diffusive scale length for individual plumes is very well specified by the standard deviation of the concentration distribution at least until this length reaches a multiple of the turbulent scale length. This multiple, however, is not well defined. We have chosen four values of Λ_D/Λ_T, ranging from one to ten, in which to investigate the sensitivity of plume growth (σ_y^2 and σ_z^2) to diffusive scale length. Keep in mind that both σ_y and σ_z are inputs to the coupled model and that, therefore, the following discussion will also provide a frame of reference when we get to the coupled model results.

Figure 6 illustrates a typical case of the diffusion history of a plume. It shows the lateral and vertical variances of the calculated distribution, σ_y^2 and σ_z^2, and the ratio of the concentration at the center of the plume to its initial value as a function of the time of travel. In a time interval of 10^5 seconds (approximately 28 hours), the plume width, as measured by σ_y and σ_z, has spread approximately two orders of magnitude in both the lateral and vertical directions, and the concentration has been diluted by a factor of 10^4. Because the lower stratosphere is stably stratified, the lateral spread is larger than the vertical spread. The degree of anisotropy as measured by σ_z^2/σ_y^2 at $t = 10^5$ is 0.2 . Although the data are not shown, the anisotropy increases (i.e., σ_z^2/σ_y^2 decreases) with increasing Ri or decreasing q^2. In fact, for $q^2 < 10^{-2}$, the diffusion is almost entirely in the lateral direction.

The change in both σ_y^2 and σ_z^2 proceeds more rapidly than t^{+1} until either σ_y^2 or σ_z^2 (or both) reaches the value of the cutoff Λ_D, which in this case is $\Lambda_D^2 = 6.2 \times 10^4$ m^2. After this point is reached, the plume spread goes over to t^{+1} in the lateral direction (a result expected from Fickian diffusion theory) and to less than t^{+1} in the vertical direction.

We could present similar plots for each of the other 19 cases which were investigated. However, we have found that all results could be conveniently summarized in one nomogram. This graphical tool not only summarizes the results but also yields the partial sensitivity of a computed parameter to each of its independent

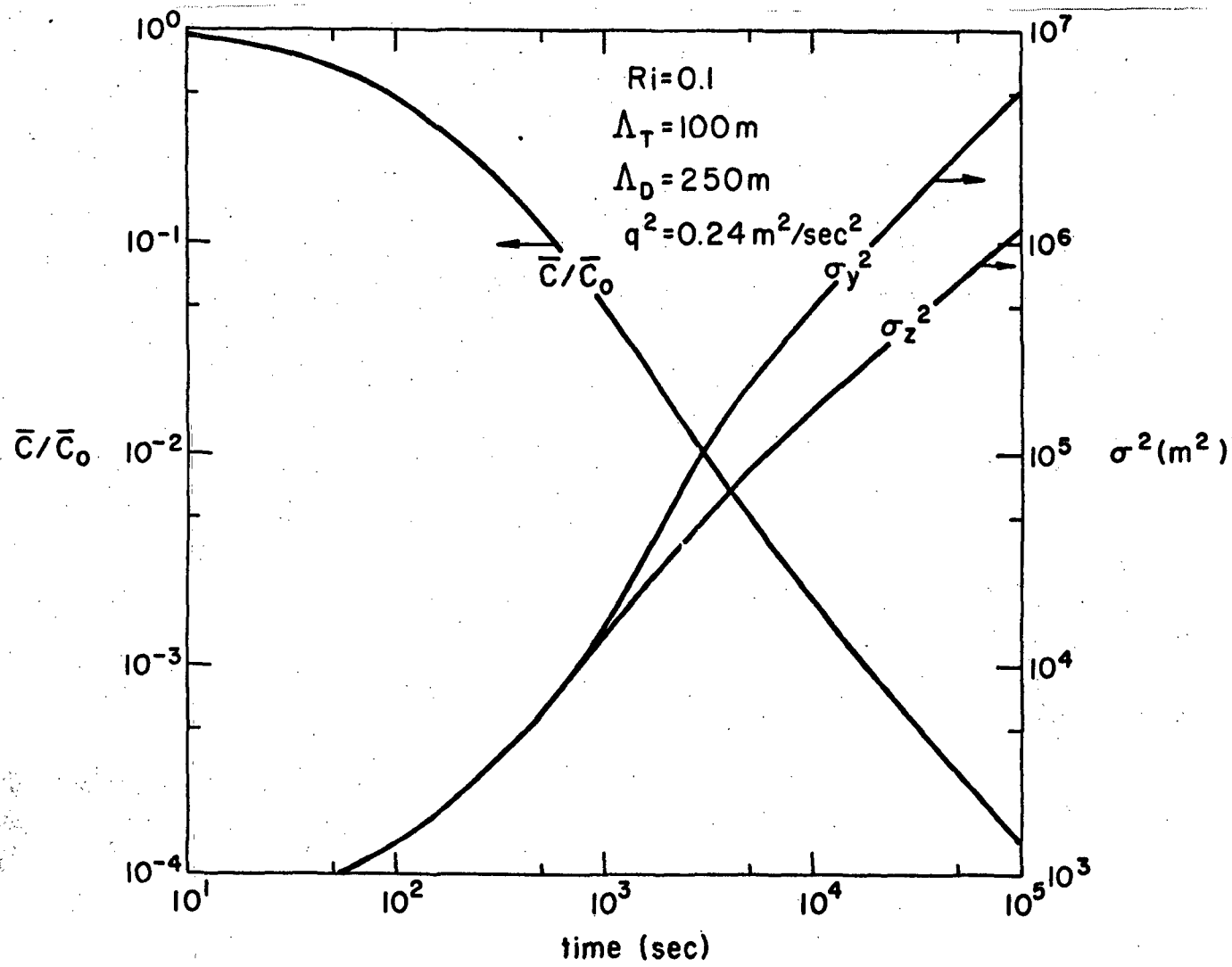

Figure 6. Illustrative example of three-dimensional diffusion history of plume. It shows the ratio of the NO concentration at the center of the plume to its initial value as well as the vertical and lateral variances of the concentration distribution for the equilibrium turbulence field defined by Ri = 0.1 and Λ_T = 100 meters.

variables. Because we will use the properties of this nomogram frequently, we will digress here and discuss its properties.

Figure 7 illustrates the generalized nomogram. Consider a dependent variable P to be a function of n dependent variables $x_1, x_2, \ldots x_n$ (where n = 4 in Fig. 7). One may easily determine the value of P for any combination of x_i by starting in the upper left quadrant with x_1 and marching around the diagram to P. For example, the variables x_1 and x_2 define a point on the $f_2(x_1, x_2)$ axis, f_2 and x_3 define a point on the $f_3(x_1, x_2, x_3)$ axis, and finally f_3 and x_4 define a value of P. If there were additional independent variables x_5, x_6, etc., one would simply continue around the diagram until the P axis was reached.

When the scales for each of the axes of the nomogram are logarithmic, the nomogram yields the partial sensitivity of P to any f_i. To demonstrate this property, assume that $f_1 = x_1$, f_2, f_3 and P are logarithmic scales in Fig. 7. Now consider the increment in P produced by an increment in x_1 as shown by the two dashed curves. If we use the definition for the slope of a line, then

$$\frac{\Delta \ell n\, f_2}{\Delta \ell n\, x_1} = S_1$$

where S_1 is the slope of the x_2 = constant curve. Note that we need not limit the analysis to straight lines if we utilize the slope of the tangent to an iso-x_2 contour. If we continue around the diagram, then

$$\frac{\Delta \ell n\, f_3}{\Delta \ell n\, f_2} = \frac{1}{S_2}$$

and

$$\frac{\Delta \ell n\, P}{\Delta \ell n\, f_3} = S_3$$

therefore,

$$\frac{\Delta \ell n\, P}{\Delta \ell n\, x_1} = \left(\frac{\Delta \ell n\, f_2}{\Delta \ell n\, x_1}\right)\left(\frac{\Delta \ell n\, f_3}{\Delta \ell n\, f_2}\right)\left(\frac{\Delta \ell n\, P}{\Delta \ell n\, f_3}\right)$$

or

$$\frac{\Delta \ell n\, P}{\Delta \ell n\, x_1} = \frac{S_1\, S_3}{S_2} \tag{28}$$

In the limit of small changes in x_1, we have

$$\frac{\partial \ell n\, P}{\partial \ell n\, x_1} = \frac{S_1\, S_3}{S_2} \tag{29}$$

where S_1, the slope of the tangent to the curve of constant x_{i+1}, is an amplification factor and $\partial \ell n\, P / \partial \ell n\, x_1$, is the

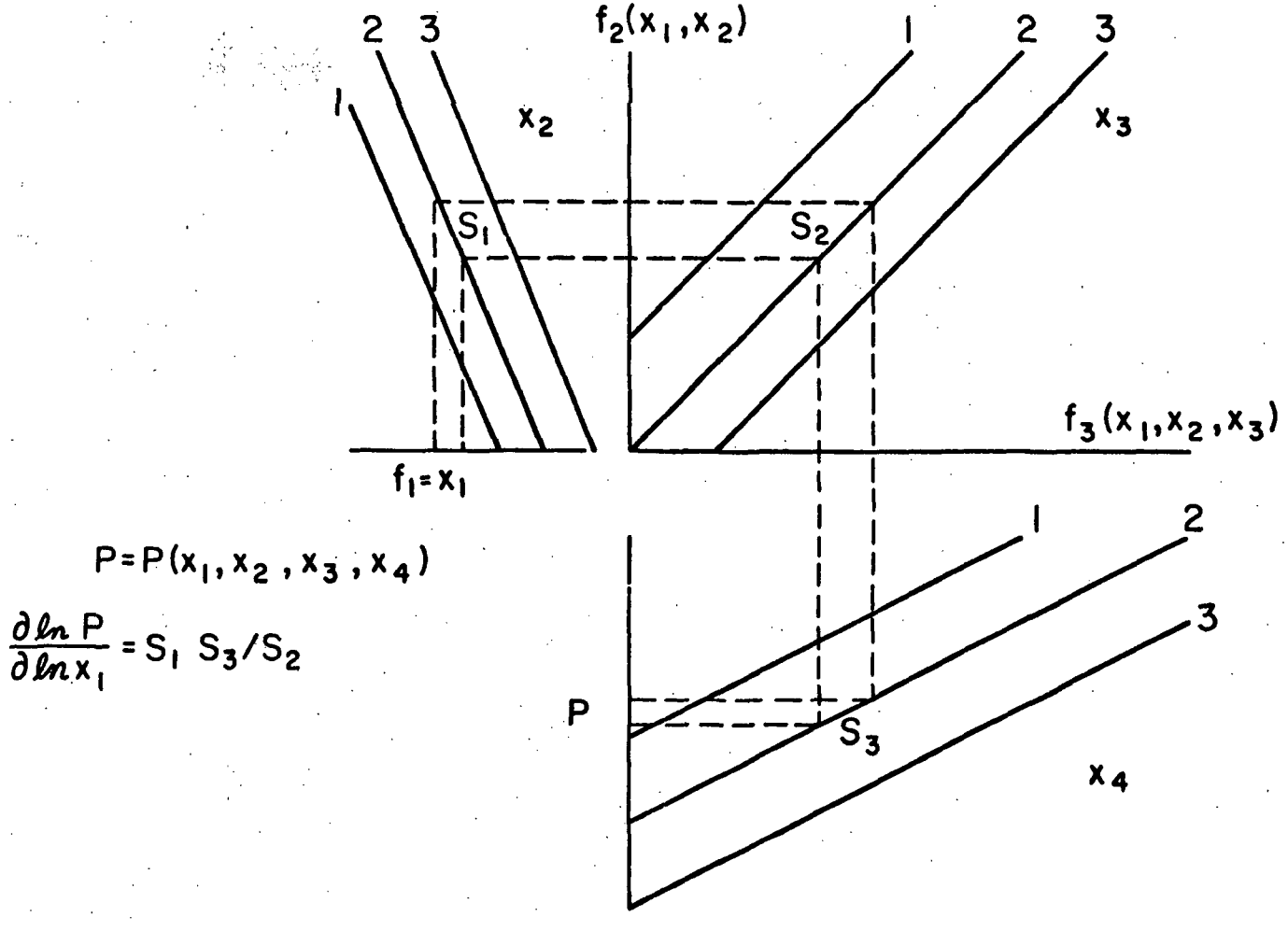

Figure 7. A generalized nomogram which shows the dependent variable P as a function of the four independent variables x_1, x_2, x_3 and x_4. The sensitivity of P to x_1 is related to the slopes of the iso-x_1 contours.

partial sensitivity of P to x_1. A similar analysis would show that the sensitivity of P to f_2 is simply

$$\frac{\partial \ell n\ P}{\partial \ell n\ f_2} = \frac{S_3}{S_2}$$

and so on for any function f_1. The final sensitivity of P to x_4 is not given directly but can be obtained by noting the incremental change in P for a change in x_4 while holding f_3 constant.

The result given by Eq. (29) can be generalized to the case of n independent variables as follows

$$\frac{\partial \ell n\ P}{\partial \ell n\ f_j} = \frac{S_1\ S_3\ S_5 \cdot \cdot \cdot \cdot}{S_2\ S_4\ S_6 \cdot \cdot \cdot \cdot} \qquad (30)$$

where $S_k = 1$ for $k \geq n$ and f_j is any transfer function ($f_j = f_1$, f_2, or f_3 in our illustration).

We can see immediately from Eq. (29) that if either S_1 or S_3 is 0 (i.e. contours of x_2 or x_4 are horizontal) or S_2 is ∞ (i.e. contours of x_3 are vertical), then x_1 will have no effect on P. If all the S_i are nonzero, then the largest value of S_i is the dominant influence on P. Finally, the algebraic sign of $S_1 S_3 / S_2$ determines whether P will increase or decrease with a given incremental change in x_1.

Nomograms which summarize the diffusion computations are shown in Figs. 8 and 9 for σ_y and σ_z respectively. The independent variables which coincide with x_1, x_2, x_3 and x_4 are Ri, Λ_T, t, and Λ_D. We can, of course, recover the results previously shown in Fig. 6. For example, if we choose Ri = 0.1 and Λ_T = 100 m, then $q^2 = f_2 = 0.24\ m^2/sec^2$, and when $t = 10^4$ sec and Λ_D = 250 m we get σ_y = 680 m.

In Fig. 8, the σ_y curves coincide for $\sigma_y \leq \Lambda_D$. Beyond the cutoff point, the plume spreads more rapidly for larger Λ_D. However, the effect of Λ_D on σ_y is significant only for relatively large turbulence intensities and for very large times. For example, when $q^2 = 0.1\ m^2/sec^2$ and $t = 10^5$ sec, σ_y = 3000 m when Λ_D = 1000 m, but σ_y is only 1000 m if Λ_D = 100 m. For a smaller $q^2 = 0.001$, the difference in σ_y is 300 m relative to 250 m for the same range of Λ_D and at the same time. For the latter intensity of turbulence, noticeable differences in plume growth due to Λ_D effects would only occur in a time scale of weeks.

The sensitivity of σ_y to Λ_D is summarized in Fig. 10 where contours of constant f_3 are shown curresponding to Fig. 8. Only when f_3 is large does Λ_D influence σ_y. When f_3 is small,

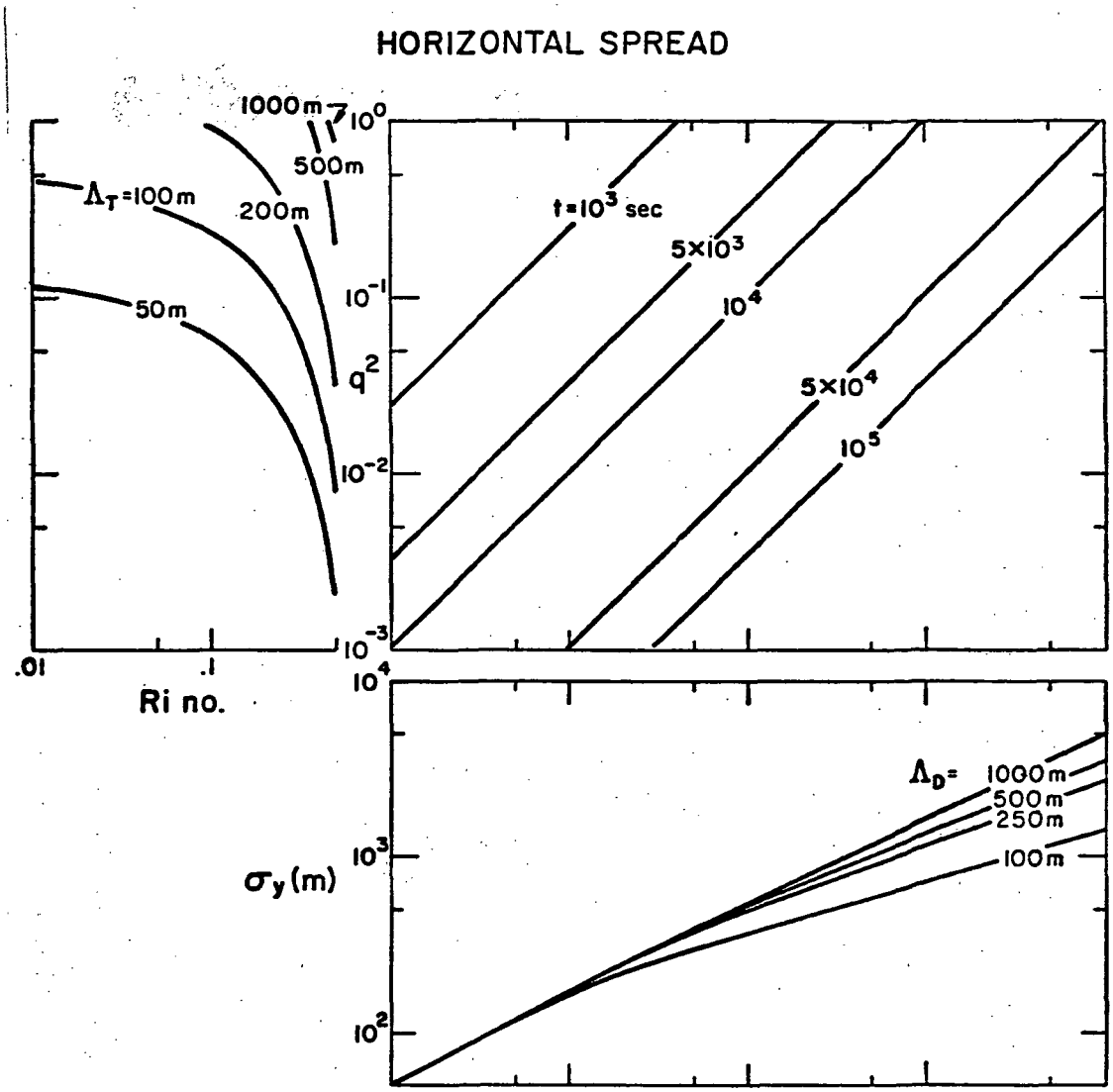

Figure 8. The dependence of the horizontal spread of the concentration distribution, σ_y, on the turbulence field (Ri and Λ_T) and the diffusive scale (Λ_D), for times after emission between 15 min. and 28 hours.

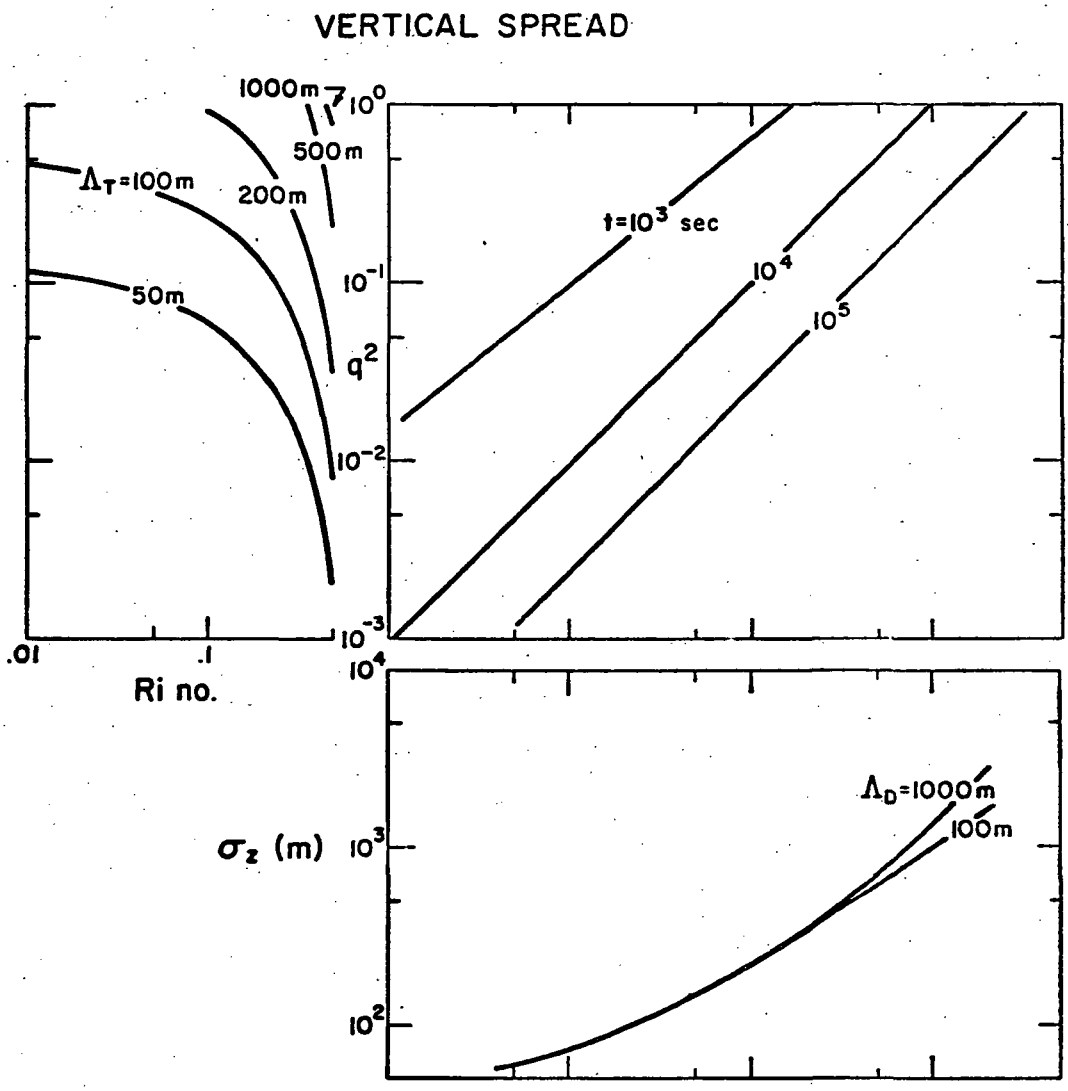

Figure 9. The dependence of the vertical spread of the concentration distribution, σ_z, on the turbulence field (Ri and Λ_T) and the diffusive scale length (Λ_D), for times after emission between 15 min. and 28 hours.

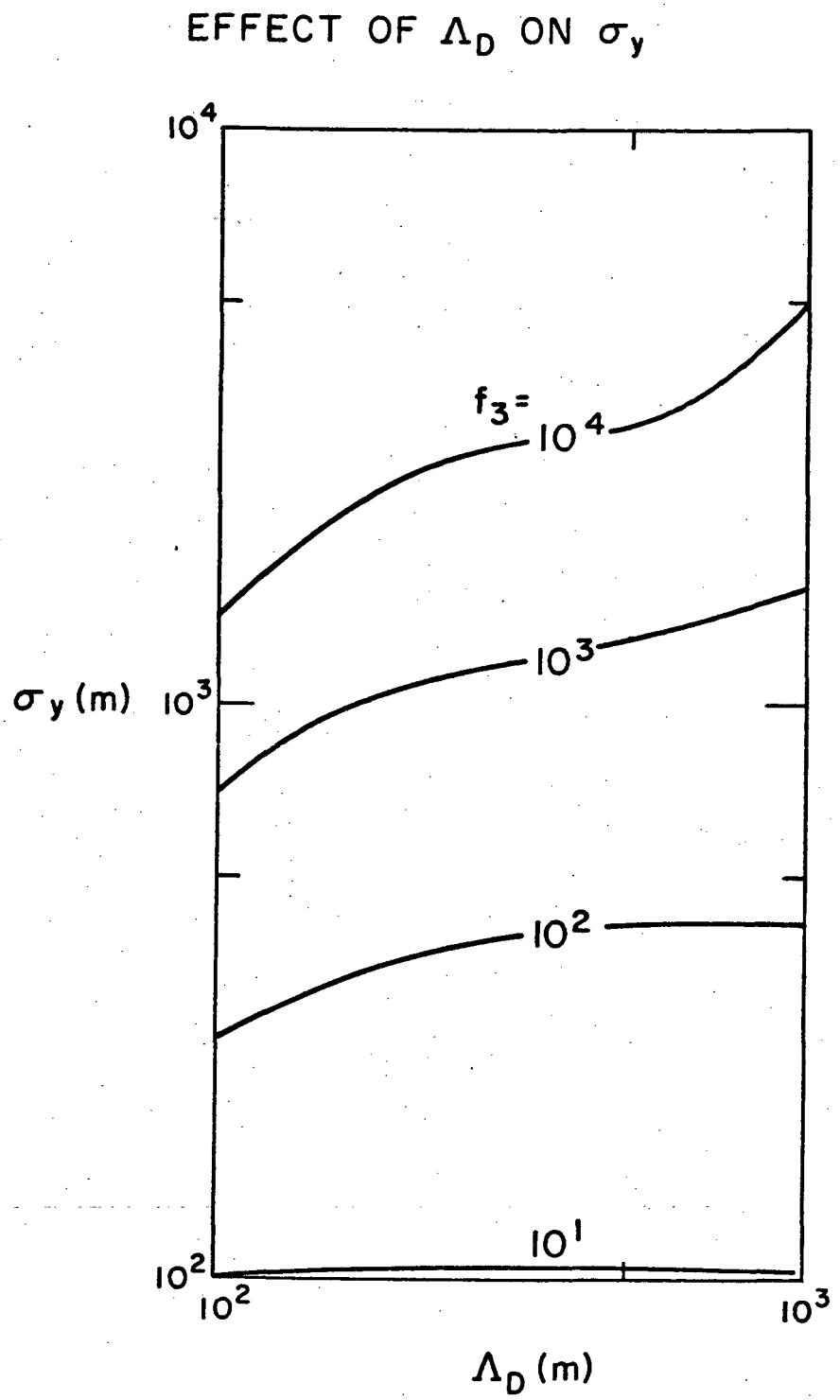

Figure 10. The sensitivity of the horizontal spread, σ_y, to the diffusive scale length, Λ_D, for four values of f_3 where f_3 is a function of Ri, Λ_T and t.

changes in Λ_D do not affect the plume spread. As noted in Fig. 8, the magnitude of f_3 increases with t and q^2.

Because of vertical stability, σ_z can be considerably smaller than σ_y. As noted in Fig. 9, the effect of Λ_D on σ_z is much smaller than was the case for σ_y.

Figures 8 and 9 demonstrate quite clearly the sensitivity of both σ_y and σ_z to the turbulence field. In particular, they demonstrate the sensitivity of σ_y (and σ_z) to Ri. We could have just as easily used $x_1 = \Lambda_T$ in our nomogram with the same results. The amplification factors (S_1, S_2, S_3 in Eq. (29)) show that the turbulence field is the critical parameter in determining the growth of the plume. For the entire domain of the diagram, $S_2 = 1$ and $S_3 < 0.5$. However, S_1 approaches $-\infty$ (the minus sign denotes a decrease in σ_y for an increase in Ri) as the stability increases and approaches the critical value. At Ri_c, of course, the diagram is no longer applicable since equilibrium turbulence cannot be sustained. Because experimental evidence does suggest high stability in the lower stratosphere, Fig. 8 (and 9) demonstrates that one had better know the turbulence before he attempts to compute the dilution time history of the plume.

In Fig. 11, we further demonstrate the importance of the turbulence intensity by showing the time required to reach a concentration dilution of 10^3, t_d. We postulate that such a dilution would be the limit of detectability of the plume and therefore t_d is a good first estimate of the duration of Phase III. It is clear that t_d is much more dependent on q^2 than on Λ_D. An order of magnitude change in q^2 also changes t_d by an order of magnitude, whereas an order of magnitude change in Λ_D changes t_d on the scale of hours. When $q^2 < 10^{-2}$ m^2/sec^2, t_d is measured in weeks and therefore Λ_d effects are insignificant. When $q^2 > 0.1$, Λ_D affects are larger but the results are really of academic interest since the plume will be completely diffused into the environment within hours anyway and furthermore the probability of sustained turbulence of that intensity is slight.

Chemical Reactions Between NO and O_3

In this analysis, we concentrate on the destruction by the NO_x catalytic cycle of only that component of O_3 which occurs in the ambient (nonplume) environment. It is recognized that the NO in an intact plume also reacts with and destroys locally produced O_3. This local production of O_3 may be high because of excessive production of O. However, the NO concentrations are also high and the locally produced O_3 is destroyed in a "do-nothing" cycle. In ref. 2, it was shown that this cycle persists until plume dilutions of 10^3 are achieved. It can therefore be assumed that there is a limiting value of the NO concentration just capable of destroying O_3 at its local production rate and any excess of NO above this level

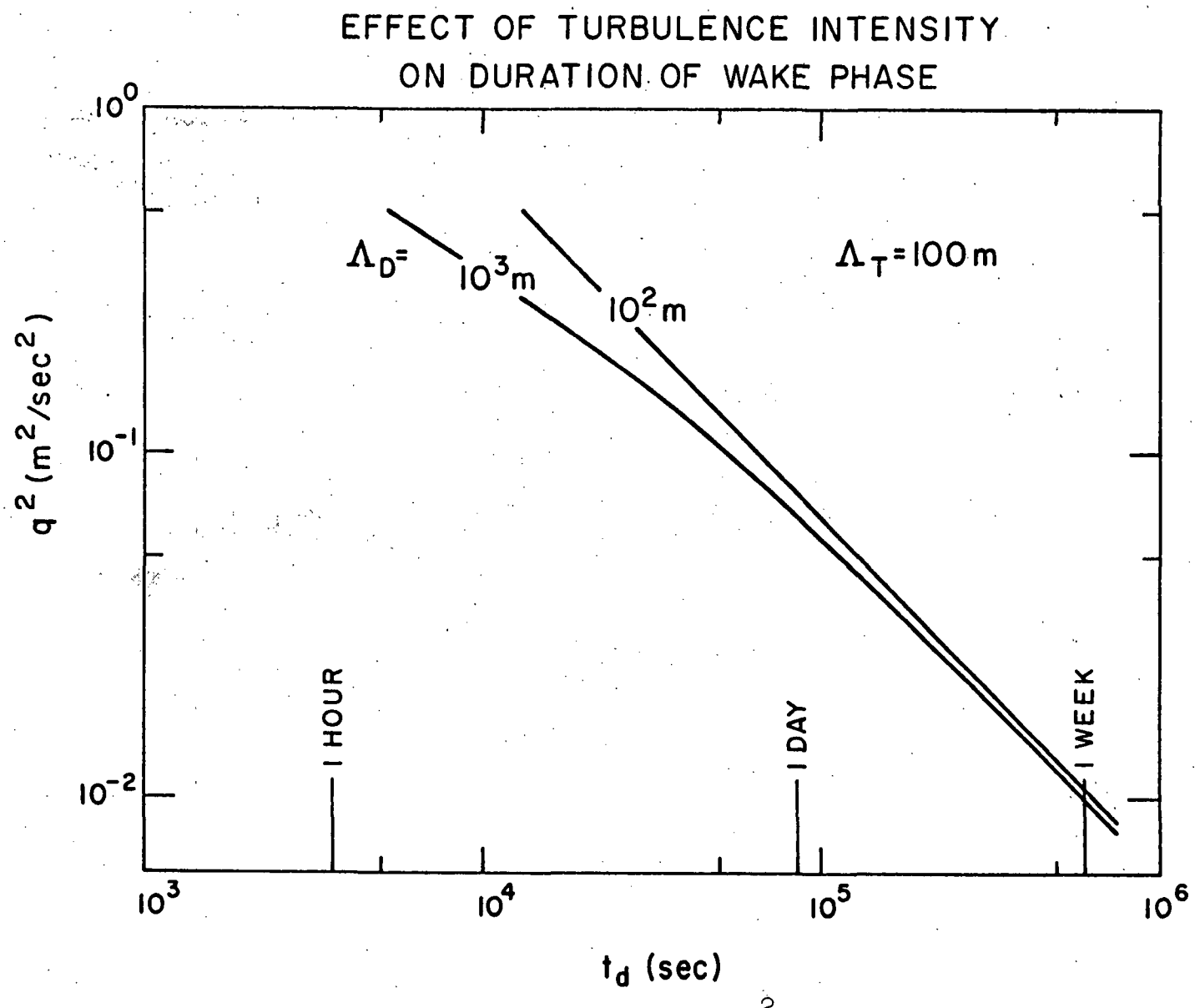

Figure 11. The effect of the turbulence intensity, q^2, and the diffusive scale length Λ_D, on the time required to achieve a concentration dilution of 10^3, t_d. This time is an estimate of the duration of the SST wake phase.

is inactive.

The depletion rate of ambient O_3 depends on the relative rates of diffusive mixing and chemical reactions. For a vertical column of unit cross-section and extending through the plume, the actual depletion rate of O_3(R) is given by

$$R = k_1 \int_{-\infty}^{\infty} (\bar{C}_\alpha \bar{C}_\beta + \overline{C'_\alpha C'_\beta}) \, dz \tag{31}$$

where α denotes the O_3 and β denotes the NO. The maximum value which $\bar{C}_\alpha$ can attain in the plume is the environmental concentration of O_3 and in this case C'_α is zero because the O_3 is uniformly distributed. The maximum depletion rate of O_3(R^*) is therefore given by

$$R^* = k_1 \bar{C}_{\alpha_e} \int_{-\infty}^{\infty} \bar{C}_\beta \, dz \tag{32}$$

where $\bar{C}_{\alpha_e}$ is the ambient concentration of O_3 and the integral is a measure of the total amount of NO in a vertical column through the plume. The chemical efficiency for any combination of NO and O_3 is then given by the ratio of Eqs. (31) and (32)

$$E = \frac{R}{R^*} = \frac{\int_{-\infty}^{\infty} (\bar{C}_\alpha \bar{C}_\beta + \overline{C'_\alpha C'_\beta}) \, dz}{\bar{C}_{\alpha_e} \int_{-\infty}^{\infty} \bar{C}_\beta \, dz} \tag{33}$$

There are two effects which prevent the reaction from proceeding at its maximum rate. First, the ambient O_3 may not be diffused into the plume rapidly enough. That is, the turbulence intensity may be too low to diffuse O_3 into the plume after the ambient O_3 in the plume is destroyed. Because there is more than enough NO to react with locally produced O_3, this means that substantial amounts of NO may be inactive until plume dilutions of at least 10^3 are achieved. It was shown in a previous section that dilution of this magnitude may not occur for days to weeks for typical turbulence intensities in the stratosphere. The diffusion limitation may be quantitatively investigated by defining the parameter, L_D, as follows

$$L_D = \frac{\bar{C}_{\alpha_e} \int_{-\infty}^{\infty} \bar{C}_\beta \, dz - \int_{-\infty}^{\infty} \bar{C}_\alpha \bar{C}_\beta \, dz}{\bar{C}_{\alpha_e} \int_{-\infty}^{\infty} \bar{C}_\beta \, dz} \tag{34}$$

In this form, L_D represents the deficit in the reaction rate due to slow diffusion of ambient O_3.

The second limitation to the maximum depletion rate is due to the mixedness term $\overline{C'_\alpha C'_\beta}$. Neglect of this term is equivalent to assuming $\overline{C}_\alpha$ and $\overline{C}_\beta$ are constant in time - a situation which certainly does not describe the real situation at least during the early stages of the reaction. Quantitatively, the mixedness limitation, L_M, is defined as

$$L_M = \frac{-\int_{-\infty}^{\infty} \overline{C'_\alpha C'_\beta}\, dz}{\overline{C}_{\alpha_e} \int_{-\infty}^{\infty} \overline{C}_\beta\, dz} \tag{35}$$

It should be noted that Eqs. (33) through (35) are simply tied together by the relation

$$E = 1 - L_D - L_M \tag{36}$$

The invariant coupled diffusion/chemistry model has been exercised in order to demonstrate the sensitivity of E (really L_D and L_M) to the various independent variables for a wide range of equilibrium turbulence fields, plume geometries, source strengths and reaction rate constants. Because the model in its present form can only handle two-dimensional diffusion, it is implicitly assumed in the following discussion that the lateral extent of the plume is large relative to the vertical extent and that lateral concentration gradients are negligible compared with the vertical. The three dimensional diffusion calculations which were described earlier demonstrate the validity of this assumption.

All of the computations are summarized in nomograms which will be discussed shortly. Because of the complexity of the computations and the number of independent variables which are involved, the information contained in the nomogram may not be immediately obvious to those who are more familiar with conventional sensitivity plots where one independent parameter is varied and all other parameters are held constant. It is therefore beneficial to describe a few of the individual computations in order to understand the underlying physics which controls the interaction between turbulent diffusion and chemical reactions and in order to set the stage for the nomograms.

Keep in mind that all coupled model computations are dynamic and that time (or more correctly for a shear flow the distance downstream of a steady line source) is a variable and the results must be qualified by stating the time regime over which the results are applicable. Figure 12 shows a typical time history of the total reaction rate as a function of the turbulence intensity. Initially, the reaction proceeds rapidly as the O_3 present in the plume reacts with the NO. While the local O_3 is being depleted, the reaction rate steadily decreases until it just balances the diffusion rate. At this time and for some time afterward, a quasi-equilibrium period exists during which turbulent diffusion provides

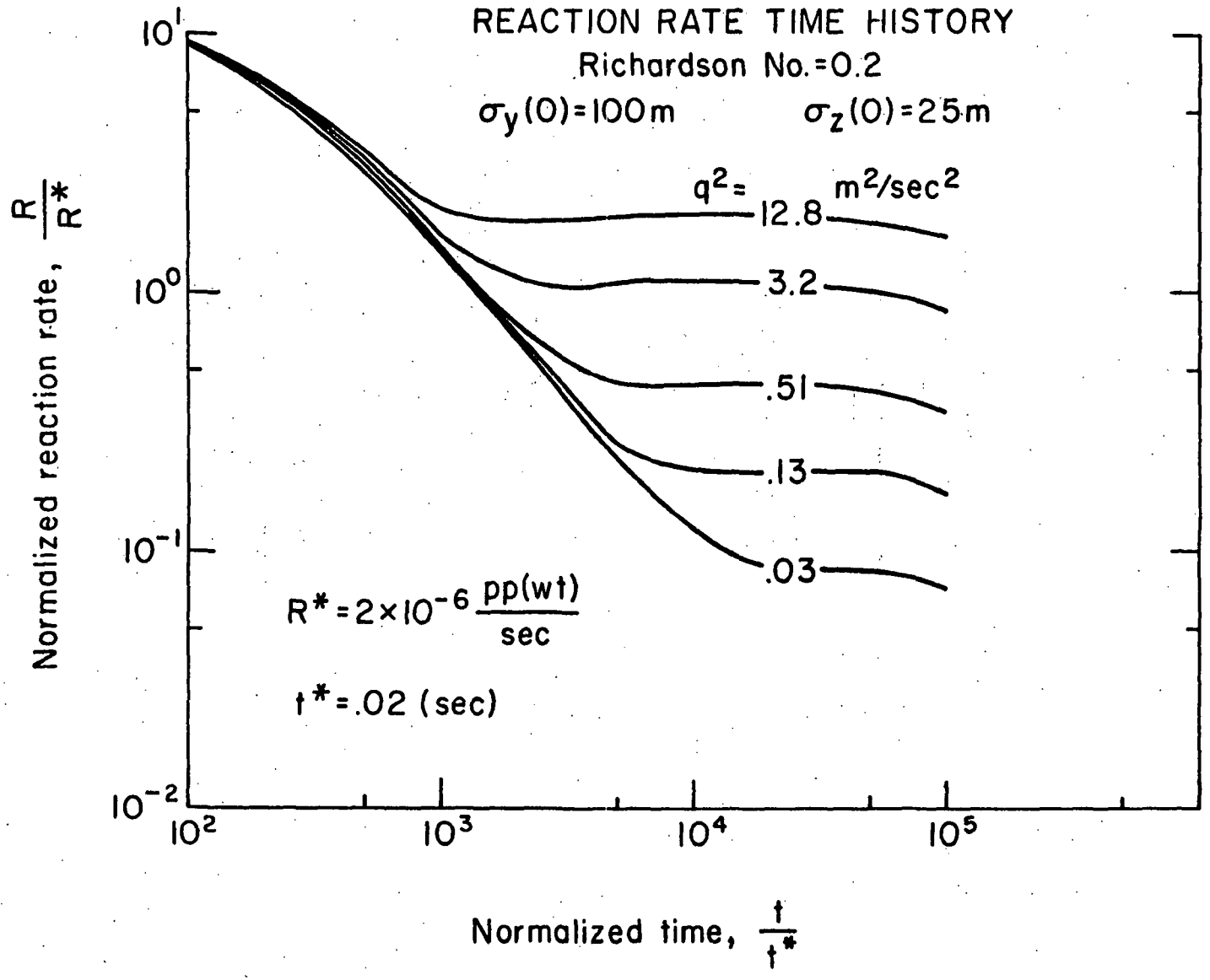

Figure 12. Typical reaction rate time histories for five values of turbulence intensity varying from 0.03 to 12.8 m^2/sec^2. R represents the integral over the vertical extent of the plume of the instantaneous local reaction rates at time t .

O_3 as rapidly as the chemical reaction depletes it. After the equilibrium period, the reaction rate drops as the result of further NO dilution.

Each computation was taken at least as far as this equilibrium period. The results presented below are for a distance of 50 km (approximately 15-30 minutes) downwind of a steady source whose initial concentration is given in Table 4 for various combinations of σ_y and σ_z. Recall that the initial concentration for the coupled model is inversely proportional to the product $\sigma_y\sigma_z$ (see Eq. (18)). Thus, the equilibrium period can be related to Phase III time using the three-dimensional diffusion nomograms described earlier. In the following paragraphs, the separate effects of turbulence, source geometry, source strength, and reaction rate constant on the species concentrations and reaction rates are described. Implicit in these results is the assumption of quasi-equilibrium.

The Turbulence Field

Consider, first, the effect of varying the turbulence field on the NO-O_3 reaction. In this discussion, the independent variables are Ri and Λ_T. The turbulence intensity, q^2, is in effect a dependent variable and is therefore not shown. We could just as easily have used Ri and q^2 as the dependent variables without changing the basic results but the resulting curves would have masked the sensitivity of the model to the turbulence scale length. The three variables are, of course, simply related for equilibrium turbulence as was shown in Fig. 2.

Figure 13 shows the effect of Ri and Λ_T on the ratio of the maximum concentration of NO to its initial value. The reduction of NO at the center of the plume is solely the result of diffusion because the NO is conserved and is unaffected by the chemistry. It is evident that diffusion proceeds more rapidly as Λ_T increases and as Ri decreases (i.e., as q^2 increases).

Figure 14 shows the effect of the same turbulence fields on the reaction rate. A two-order of magnitude increase in the reaction rate can be observed as the turbulence field varies from highly stable, small scale eddies to neutrally stable, large scale eddies.

Figure 15 shows the O_3 concentration at the center of the plume. It is evident that when the turbulent diffusion rate is low the O_3 concentration can be more than three orders of magnitude lower than its ambient value. In other words, a portion of the plume is essentially free of O_3 - a region which is termed the "O_3 - hole". The presence of the O_3 hole has a detrimental effect on the chemical efficiency because all of the NO present in the hole (and keep in mind the hole is at the center of the plume where the NO concentration is a maximum) is unreactive.

The extent of the O_3 hole can be quantitatively estimated if one is willing to arbitrarily define a concentration level below

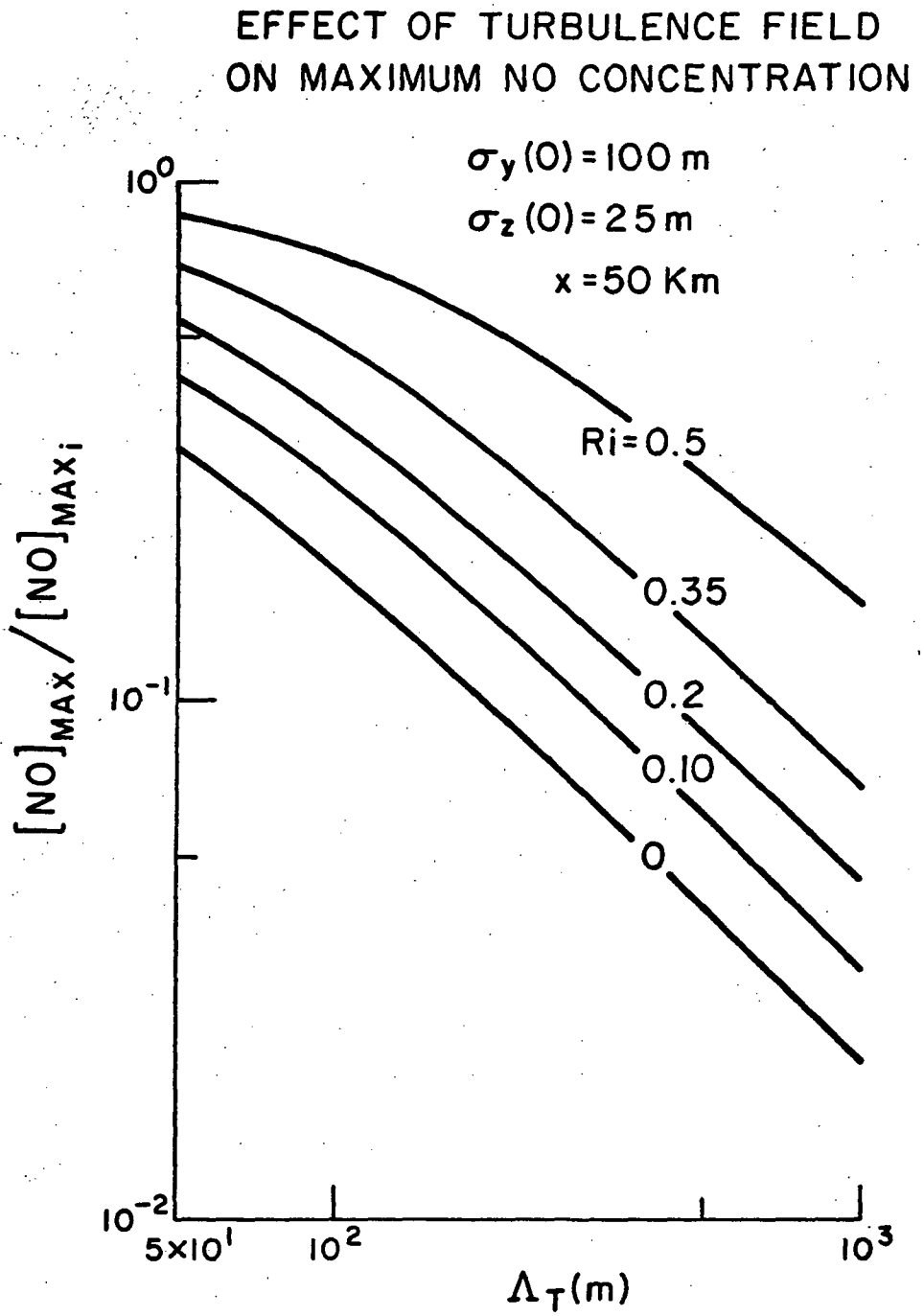

Figure 13. Typical effect of the turbulence field, (as defined by Ri and Λ_T), on the ratio of the NO concentration at the center of the plume to its initial value. The initial plume geometry ($\sigma_z(0)$ = 25 m and $\sigma_y(0)$ = 100 m) is fixed.

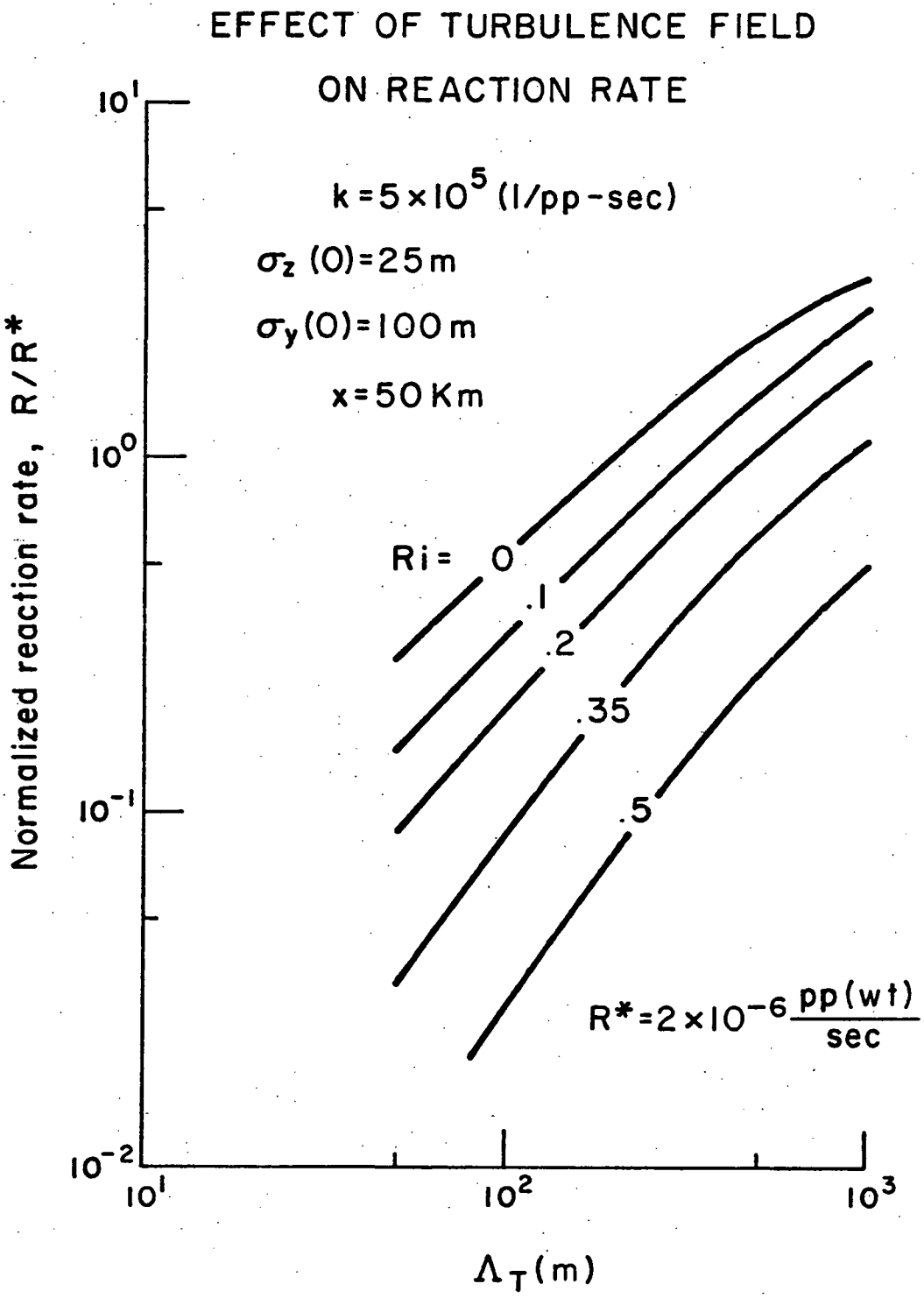

Figure 14. Typical effect of the turbulence field on the total depletion rate of ambient O_3. The initial plume geometry is the same as for Fig. 13 and the reaction rate constant is $k = 5 \times 10^5 (\text{pp-sec})^{-1}$.

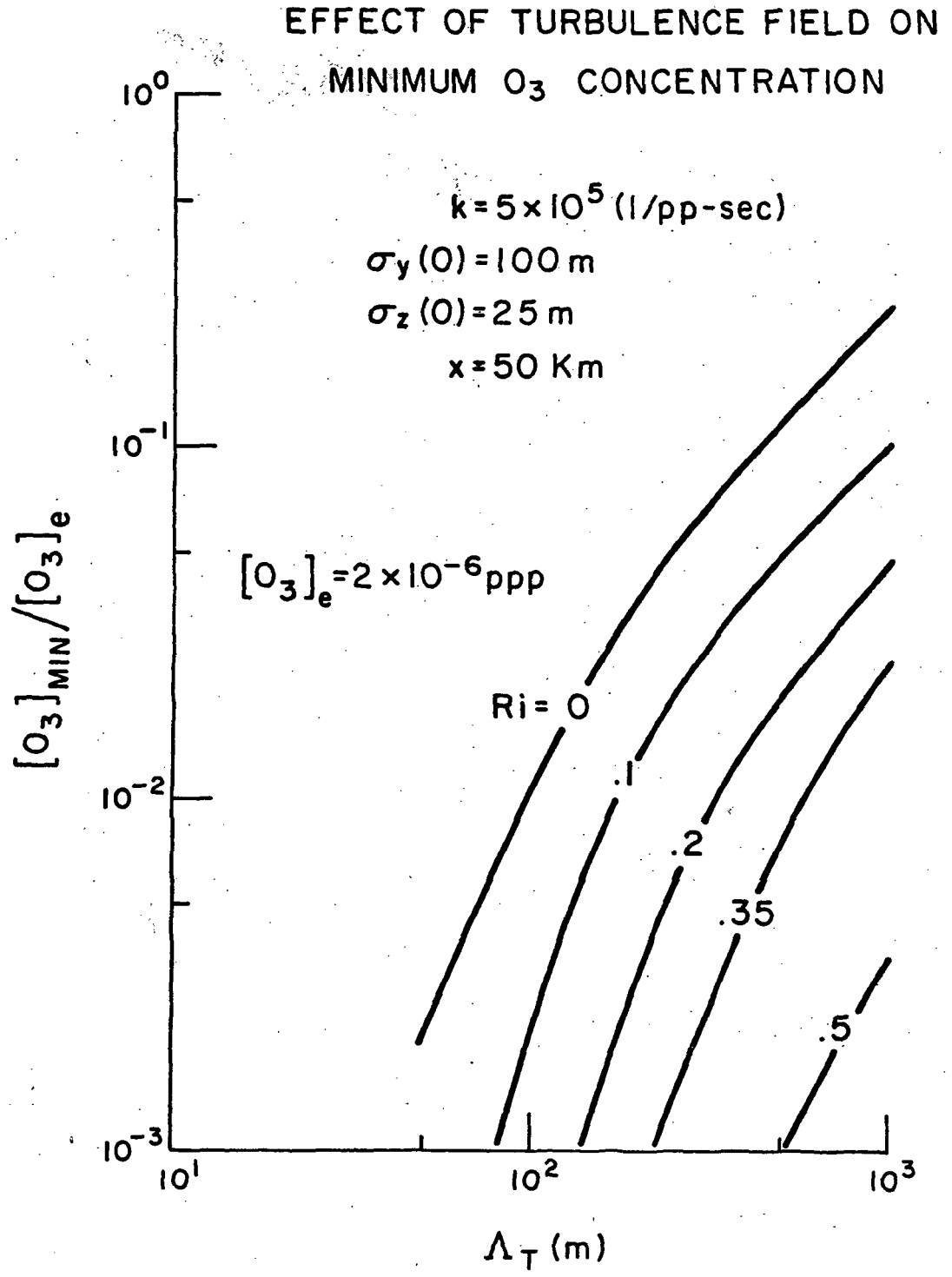

Figure 15. Typical effect of the turbulence field on the O_3 concentration at the center of the plume for the same conditions as for Fig. 14.

which the O_3 concentration is effectively zero. For purposes of discussion, if we define this level as 10^{-3} times the ambient concentration, then Fig. 16 shows the maximum thickness of the O_3 hole which is developed. For very stable and small-scale turbulence, the thickness of the hole can be more than 100 meters or nearly equal to the initial thickness (i.e., $4\sigma_z$) of the plume.

Plume Geometry

The effect of plume geometry was investigated by varying both σ_y and σ_z. Because only vertical diffusion is considered, the lateral extent of the plume is, in effect, a measure of the source strength as was noted earlier in Eq. (23). We will, therefore, postpone the σ_y discussion until the next section and consider only σ_z in this section.

Figure 17 shows the effect of σ_z on the maximum NO concentration for five turbulence fields. For a fixed source strength, the concentration gradient $(\partial\overline{C}/\partial z)$ decreases as σ_z increases and, therefore there is less diffusion of NO from the center of the plume for the larger values of σ_z.

Figure 18 shows the O_3 concentrations at the center of the plume as a function of σ_z for three turbulence fields. For a neutrally stable environment, the O_3 concentration slowly decreases as σ_z increases. As the stability increases, the balance between the reaction rate and the diffusion rate shifts and the sensitivity of O_3 concentration to σ_z increases. Although the sensitivity is increasing with Ri, the concentration levels are 10^{-3} to 10^{-5} times the ambient value and therefore we can anticipate that these results will have a minor influence on the chemical efficiency.

Figure 19 shows the effect of σ_z on the total reaction rate for the same three turbulence fields as Fig. 18. For the most part, the reaction rate is insensitive to σ_z and never varies by more than 20% for a factor of four change in σ_z. Again, these results suggest that σ_z will have a negligible effect on the chemical efficiency.

Source Strength

Figure 20 shows that the normalized maximum concentration of NO is independent of source strength or, in other words, the maximum local concentration of NO varies directly as the amount of NO emitted at the source. This is not surprising because the NO is conserved and the initial concentration is directly proportional to the source strength.

The source strength has a significant effect on the O_3 concentration at the center of the plume as shown in Fig. 21. For a fixed turbulence field, as the amount of NO is increased (i.e. σ_y

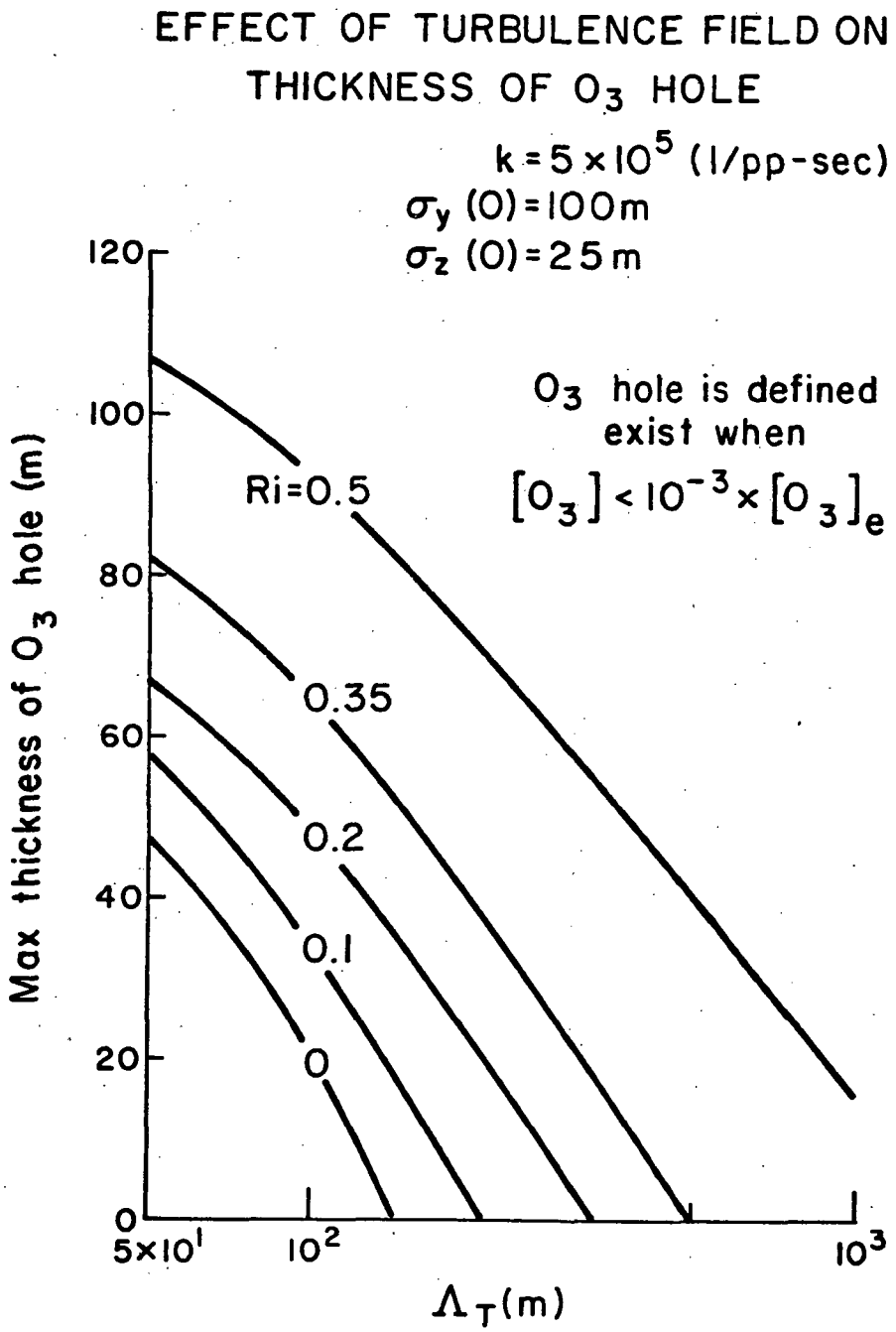

Figure 16. The effect of the turbulence field on the maximum vertical thickness of the O_3-hole for the same conditions as for Fig. 14. The O_3-hole is defined as the region around the center of the plume within which the O_3 concentration is less than 10^{-3} times the ambient O_3 concentration of 2×10^{-6} ppp.

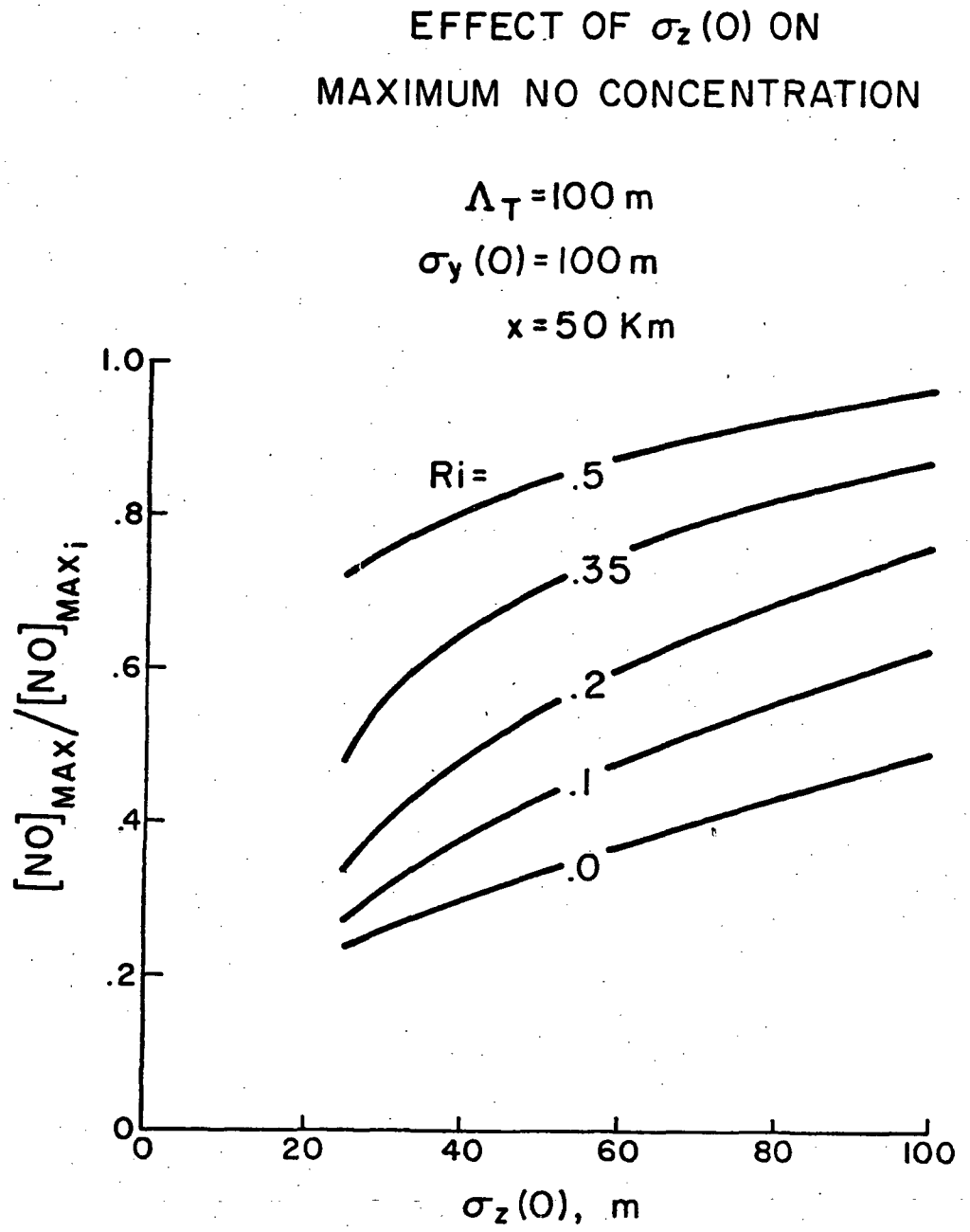

Figure 17. *Typical effect of* $\sigma_z(0)$ *- the initial vertical spread of the NO concentration distribution -* on the ratio of the NO concentration at the center of the plume to its initial value for five values of Ri . The parameters Λ_T , $\sigma_y(0)$, and x are held fixed at 100 m , 100 m , and 50 km respectively.

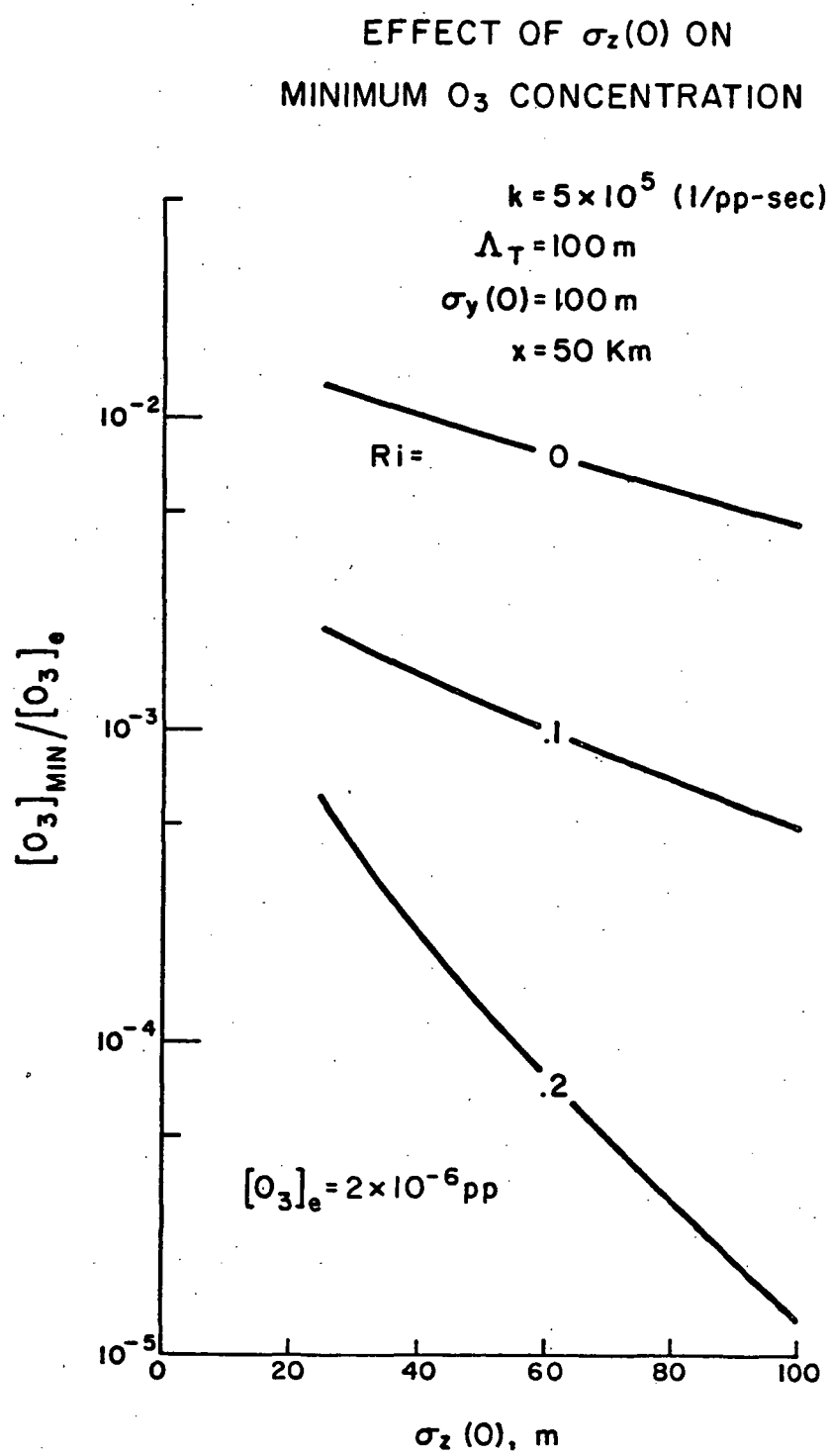

Figure 18. Typical effect of $\sigma_z(0)$ on the O_3 concentration at the center of the plume for three values of Ri. The parameters Λ_T, $\sigma_y(0)$, and x have the same values as for Fig. 17 and, in addition, $k = 5 \times 10^5$ $(pp\text{-}sec)^{-1}$.

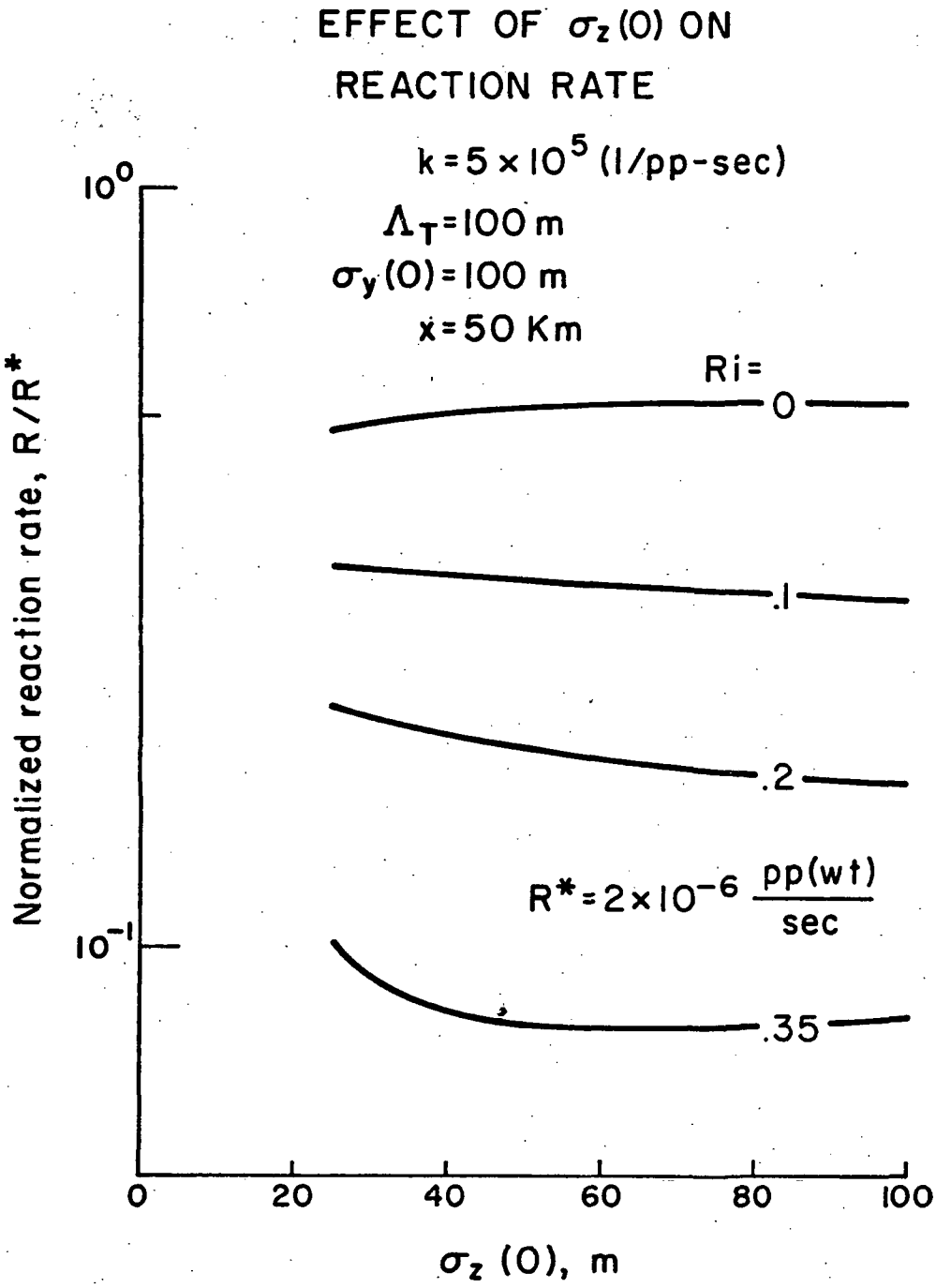

Figure 19. Typical effect of $\sigma_z(0)$ on the total depletion rate of ambient O_3 for the same conditions as for Fig. 18.

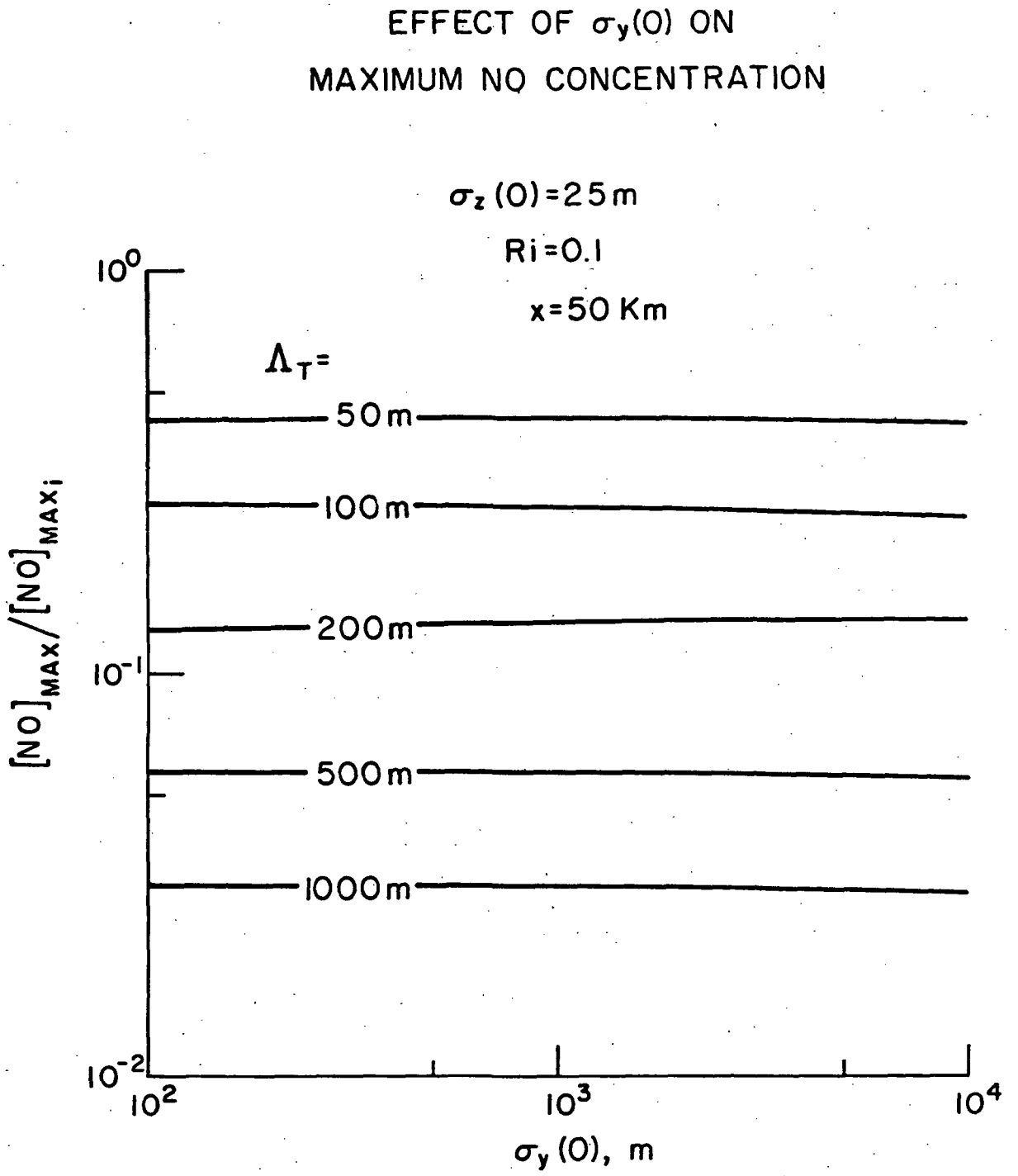

Figure 20. Typical effect of $\sigma_y(0)$ - the initial lateral spread of the NO concentration distribution - on the ratio of the NO concentration at the center of the plume to its initial value for five values of Λ_T . The parameters Ri , $\sigma_z(0)$, and x are held constant at 0.1, 25 m , and 50 km respectively. For two-dimensional diffusion, $\sigma_y(0)$ is inversely proportional to the source strength.

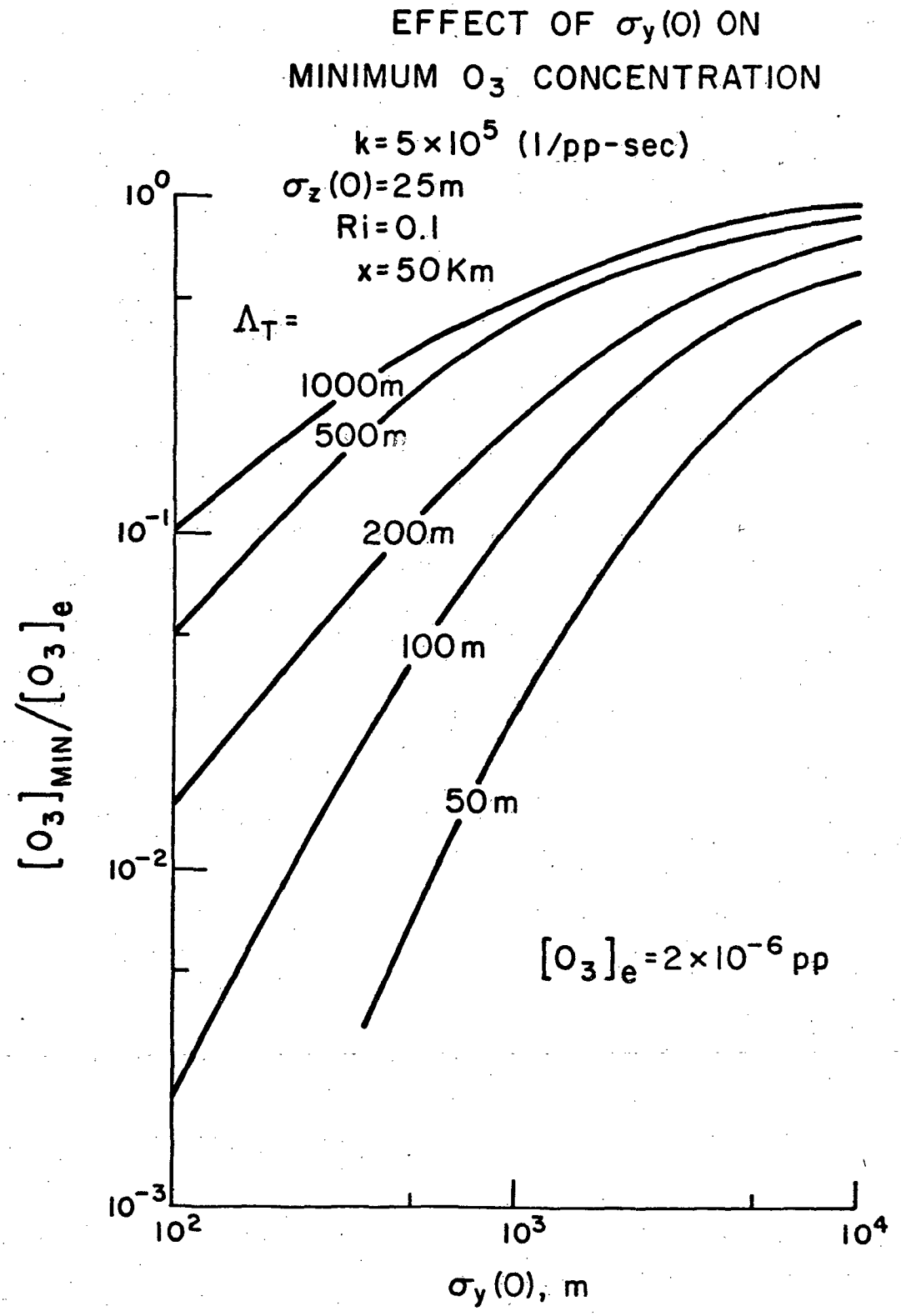

Figure 21. Typical effect of $\sigma_y(0)$ on the O_3 concentration at the center of the plume for the same conditions as for Fig. 20 and for $k = 5 \times 10^5 (pp\text{-}sec)^{-1}$.

decreases) the total reaction rate increases and therefore the O_3 concentration decreases. The sensitivity of $[O_3]_{min}$ to σ_y increases as the turbulence intensity (i.e., Λ_T) decreases because the O_3 is less able to penetrate deep into the plume. That is to say, the increased sensitivity illustrates the tendency for the reaction to become diffusion limited for low turbulence intensity.

Figure 22 shows the effect of source strength on the reaction rate. For very dilute plumes, the reaction rate should be linearly dependent on the amount of NO present in the plume. The curves shown in Fig. 22 appear to be approaching this linear dependence on σ_y for $\sigma_y > 10^4$. As the amount of NO is increased ($\sigma_y < 10^4$), the reaction rate departs considerably from a linear dependence due to diffusion and mixedness limitations. That is to say, diffusion and mixedness are becoming increasingly important in controlling the total reaction rate. For example, a tenfold increase in the amount of NO (from $\sigma_y = 10^3$ to $\sigma_y = 10^2$) in a turbulence field whose $q^2 = .06\ m^2/sec^2$ ($\Lambda_T = 50$ m) results in a negligible increase in the reaction rate. This is because the diffusion rate is extremely slow, the reaction is occurring at the edges of the plume and the bulk of the NO has no O_3 with which to react.

Reaction Rate Constant

The reaction rate constant for the depletion of O_3 was varied through four orders-of-magnitude. Because the NO is conserved, k has no effect on the NO concentration. It does have, however, a pronounced effect on the O_3 concentration at the center of the plume as shown in Fig. 23 and on the reaction rate as shown in Fig. 24.

In each figure, for large values of k both the minimum O_3 concentration and the reaction rate are strongly dependent on the turbulence intensity. That is to say, the reaction is tending toward the diffusion limitation. For small values of k, the reaction is nearly independent of the turbulence intensity and proceeds at a rate controlled by k. The reaction is now slow enough so that turbulent diffusion can supply all of the O_3 needed to react with the NO and, in fact, the O_3 concentration doesn't vary by more than a factor of two across the plume. Note in Fig. 23, that a tenfold decrease in k from 5×10^5 to 5×10^4 practically eliminates the O_3-hole. Also note, this time in Fig. 24, that the total reaction rate increases as k^n and that $n = +1$ for small k and that n decreases steadily with increasing k. We would expect, therefore, that the chemical efficiency would decrease with increasing k because the maximum possible reaction rate is everywhere proportional to k^1.

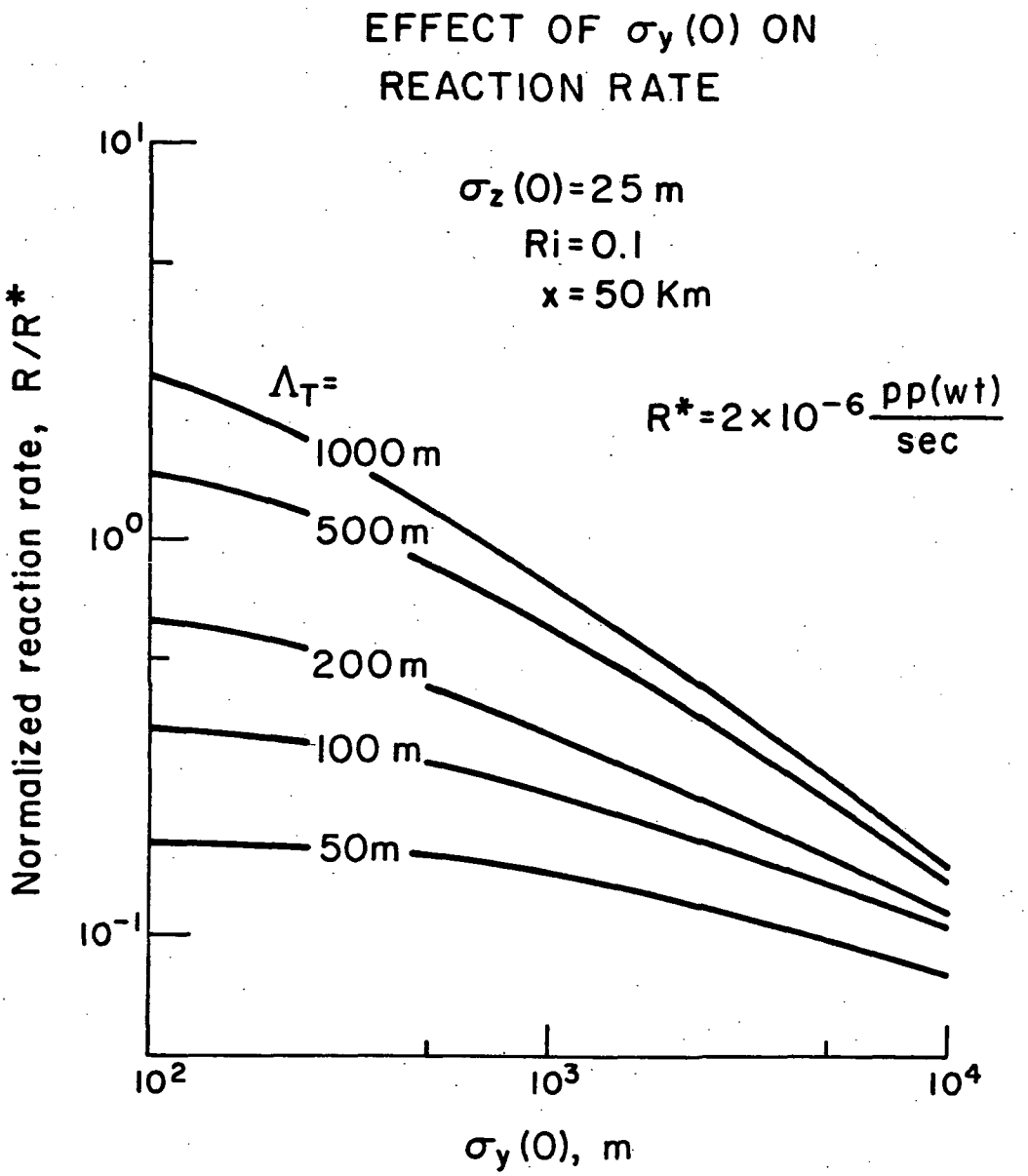

Figure 22. Typical effect of $\sigma_y(0)$ on the total depletion rate of ambient O_3 for the same conditions as for Fig. 21.

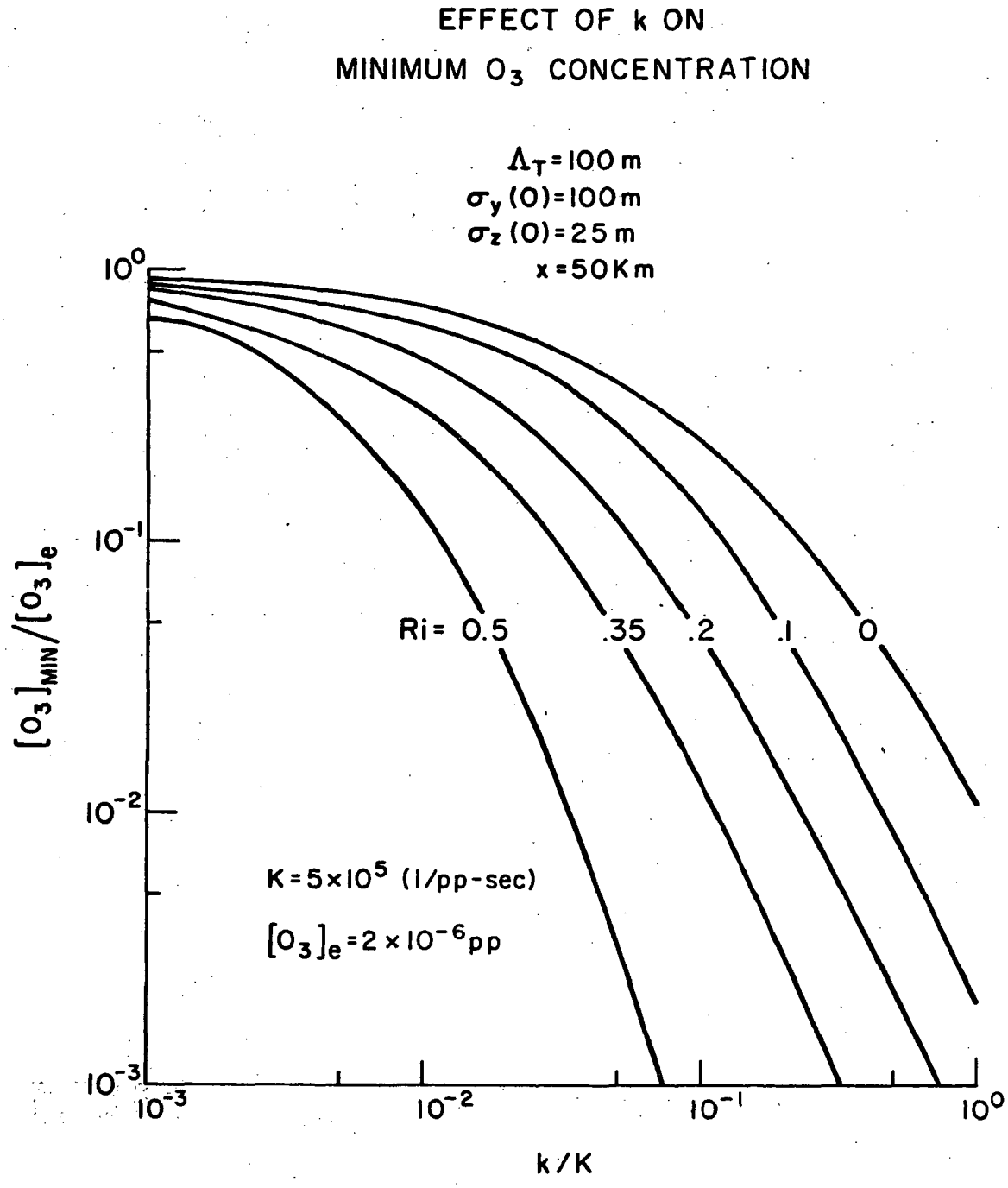

Figure 23. Typical effect of the reaction rate constant on the O_3 concentration at the center of the plume for five values of Ri . The other parameters are held constant; Λ_T = 100 m , $\sigma_z(0)$ = 25 m , $\sigma_y(0)$ = 100 m, and x = 50 km.

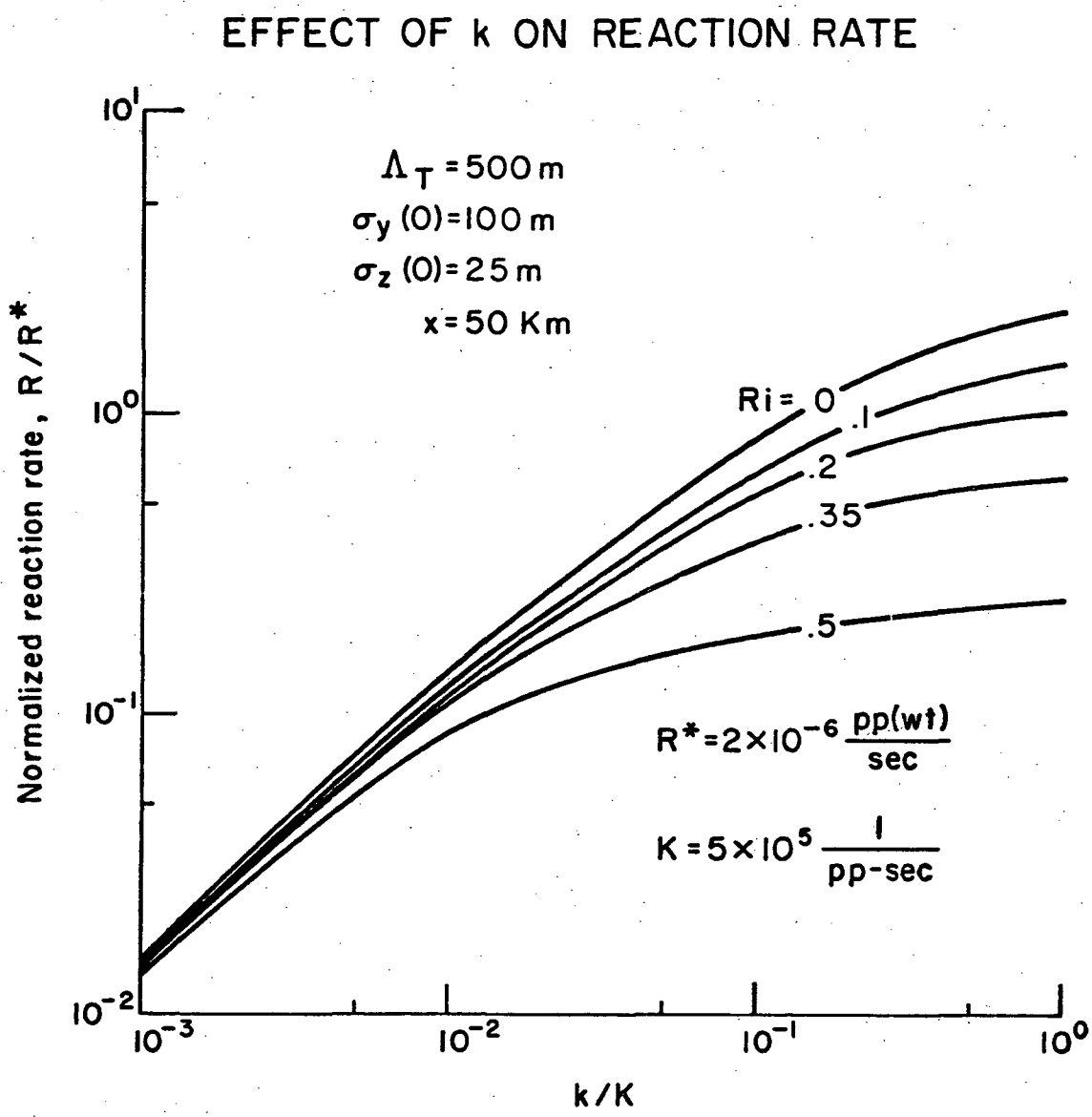

Figure 24. Typical effect of the reaction rate constant on the total depletion rate of ambient O_3 for the conditions Λ_T = 500 m , $\sigma_z(0)$ = 25 m , $\sigma_y(0)$ = 100 m and x = 50 m.

Chemical Efficiency

The results described above can be recast in terms of the chemical efficiency (E) and in terms of the diffusion and mixedness limitations (L_D and L_M, respectively) which act independently to limit E to values less than one. In an earlier section, each of these terms was defined (Eqs. (33)-(35)).

One might well recall, at this point, the implications of the chemical efficiency as far as the O_3 inventory in the stratosphere is concerned. In Ref. 2, we showed that the average chemical efficiency for the entire residence time of the plume $\bar{E}(T_R)$ is given by

$$\bar{E}(T_R) = 1 - \frac{T}{T_R}(1 - E) \qquad (37)$$

where T is the duration of Phase III and T_R is the residence time of the plume in the stratosphere. Clearly, as $T/T_R \rightarrow 1$, $\bar{E}(T_R) \rightarrow E$ and E, therefore, is a measure of the overall effect of Phase III chemistry limitations on the theoretical depletion rate of environmental O_3 due to the SST. Of course, if $T/T_R \rightarrow 0$ or $E \rightarrow 1$, then $\bar{E}(T_R) \rightarrow 1$ and Phase III chemistry effects are of academic interest. Present best estimates of T/T_R vary from less than 0.1 to as much as 0.5 and as will be shown below E can vary from less than 0.01 to 0.99. Thus, Phase III chemistry limitations can have a significant influence on the O_3 inventory in the stratosphere.

The chemical efficiency nomogram is presented in Fig. 25. The independent variables are Ri, Λ_T, σ_y and k. All of the data in Fig. 25 are for $\bar{\sigma}_z = 50$ meters. Before we discuss these results, we should note that E is relatively insensitive to σ_z.

The effect of σ_z on E is shown in Fig. 26. A band is shown for each of three values of σ_y. The upper value of the band usually corresponds to $\sigma_z = 100$ m and the lower value to $\sigma_z = 25$ m. For dilute plumes, σ_z is seen to be a relatively small effect in comparison to changes in σ_y. For compact plumes, the spread is larger but the differences are between a fraction of 1% and 3% - differences which are of little consequence. We, therefore, omit σ_z from further discussion and note that, strictly speaking, all of the following results are for $\sigma_z = 50$ m.

Let us return to Fig. 25 in which some of the results described earlier are clearly evident. When the turbulence intensity is high and σ_y is large, E approaches unity no matter what the reaction rate constant. In contrast, when q^2 is low and the plume is compact k is an extremely important parameter and the efficiency can vary from 80% for slow reactions to less than 1% for very fast reactions.

In the context of our earlier discussion of the nomogram, the slopes of the curves in Fig. 25 amplify the sensitivity of E to

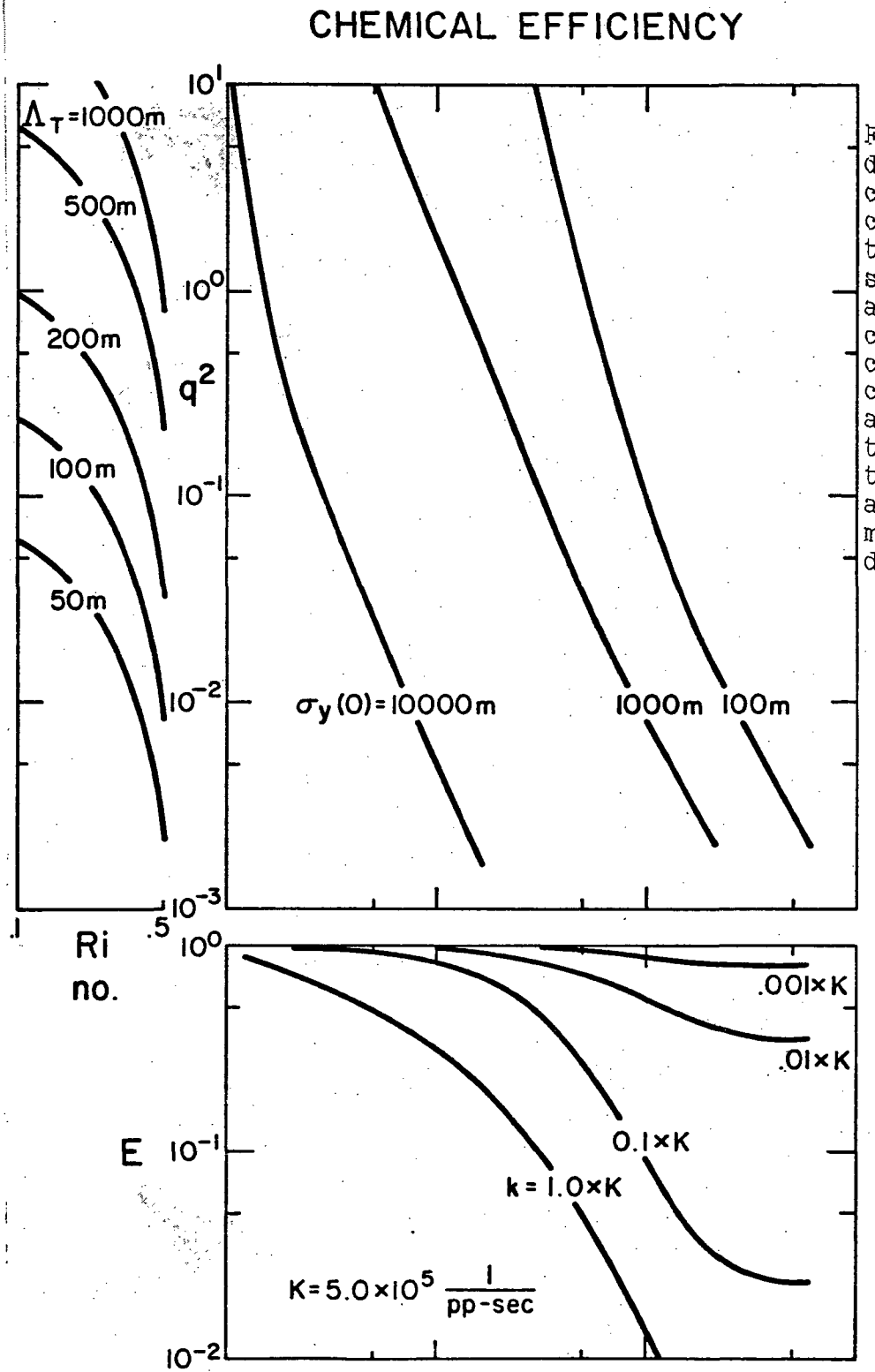

Figure 25. The dependence of the chemical efficiency on the turbulence field, source strength, and reaction rate constant. The chemical efficiency is defined as the ratio of the actual depletion rate of ambient O_3 to the maximum possible depletion rate.

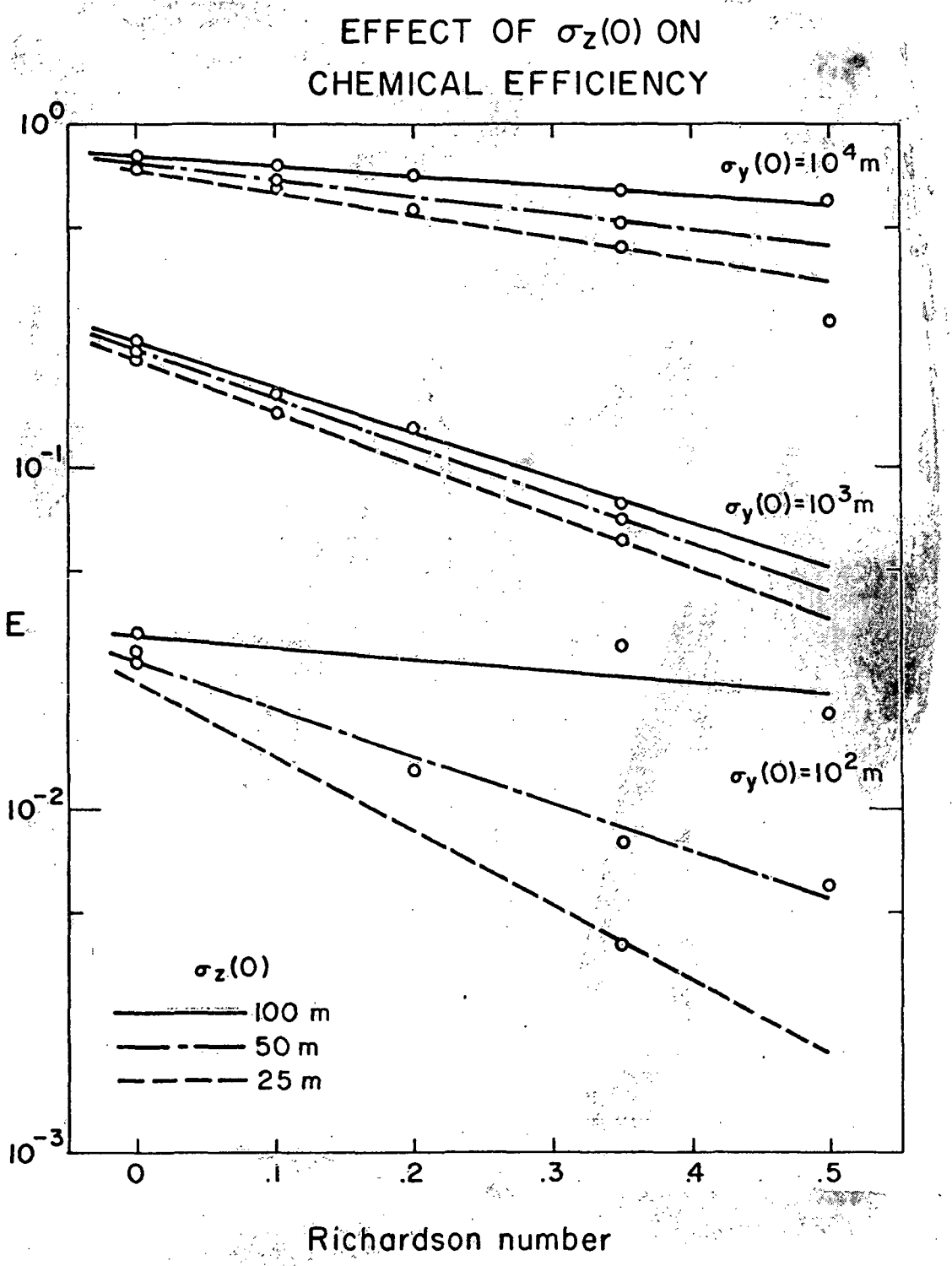

Figure 26. The effect of $\sigma_z(0)$ - the initial vertical spread of the NO concentration distribution - on the chemical efficiency for three values of $\sigma_y(0)$.

the Ri . The slope of the iso-Λ_T contours (S_1) increases rapidly as the Ri approaches the critical Ri of 0.55. Thus E is most sensitive to the turbulence field when the stratosphere is highly stable. The slope of the iso-σ_y contours is nearly constant for q^2 less than 0.1 and therefore the sensitivity of E to the turbulence field is relatively independent of plume geometry. For very large q^2 , S_2 approaches infinity and E becomes independent of the turbulence. However, this result is mainly of academic interest because sustained turbulence in excess of 10 m^2/sec^2 in the stratosphere is highly unlikely. The slope of the iso-k contours (S_3) is maximum for intermediate values of the transfer function f_3. For large values of f_3 (i.e. very compact plumes), S_3 approaches 0 and E becomes independent of Ri and varies only with k . Thus, E is most sensitive to the turbulence field when the flow field is highly stable, the reaction rate is fast and the plume is moderately diffused.

The partial sensitivity of E to σ_y is illustrated in Figs. 27-29 for three values of the turbulence intensity and three values of k . The three figures clearly show that:

1) E increases strongly with σ_y or, in other words, the less NO emitted per unit distance of travel the more efficient the destruction of O_3 .

2) E is most sensitive to σ_y when the NO concentrations are high. As the plume becomes diffused, the sensitivity to σ_y decreases.

3) The sensitivity of E to σ_y decreases as k decreases. Figure 29 shows that E is always above 40% when $k = 5 \times 10^3$ (1/pp-sec). In this case, conventional mean-value chemistry would predict the depletion of O_3 to within a factor of two.

The sensitivity of E to k is illustrated in Fig. 30 in which lines of constant f_3 are shown. Recall that f_3 is a transfer function of Ri, Λ_T and σ_y and that for increases in each of these variables f_3 increases with Ri and decreases with Λ_T and σ_y . When the reaction rate constant is very small, E is nearly unity no matter what the value of Ri , Λ_T and σ_y . As k increases, the reaction becomes more diffusion and mixedness limited and the efficiency decreases. For very large values of f_3, the iso-f_3 contours tend to merge and E becomes a function of k only.

In order to put all of the above results in perspective, we can illustrate the importance of each of the independent variables by citing a typical example. For purposes of discussion, assume that a typical condition in the lower stratosphere is given by $q^2 = 10^{-2} m^2/sec^2$, $\sigma_y = 10^3 m$, and $k = 5 \times 10^4$ (1/pp-sec) . For these conditions, Fig. 25 shows that E = 10% and we can ask the question, how much does E change if each of the variables is changed independently by one order of magnitude? Table 7 summarizes the answer to this question.

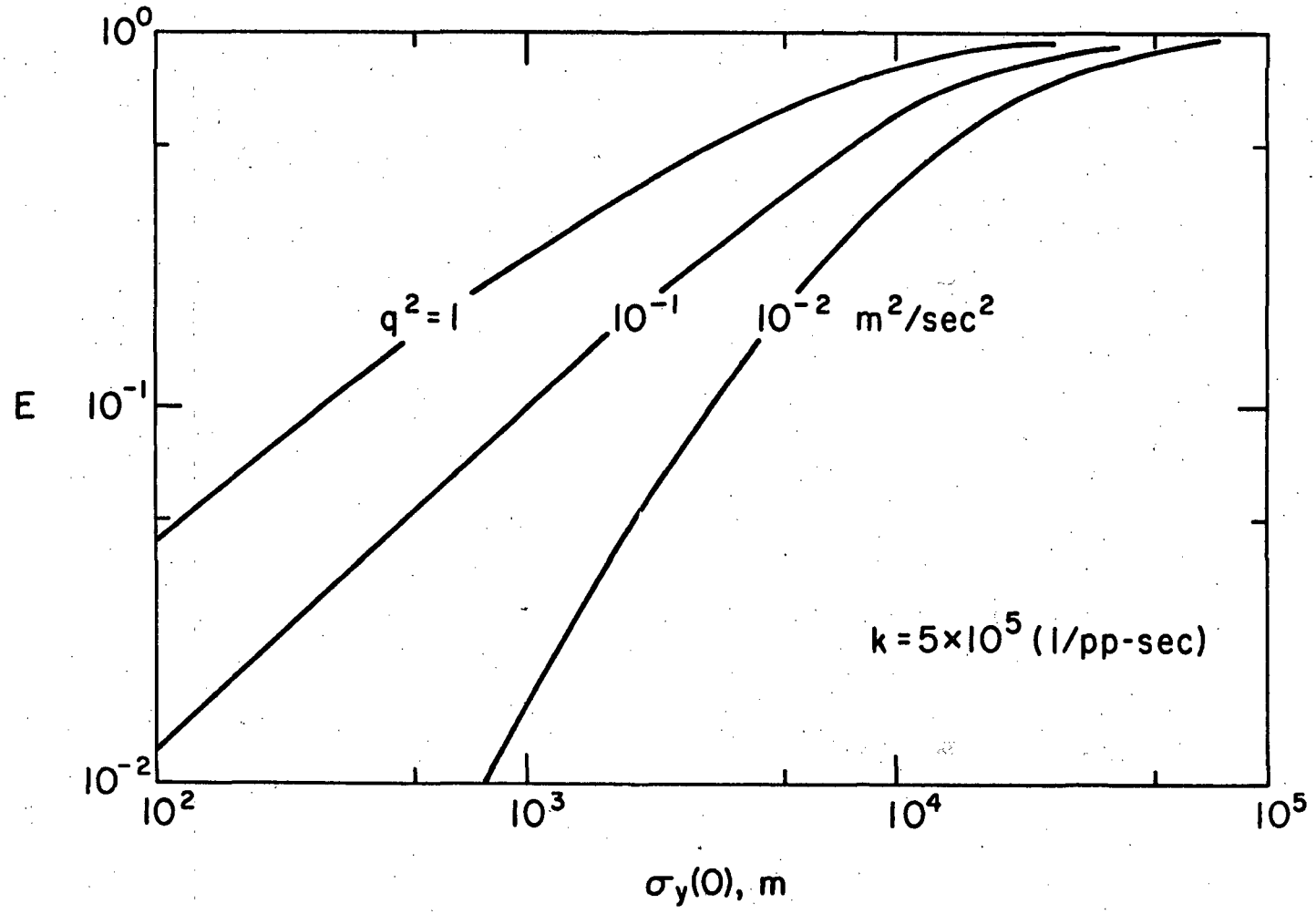

Figure 27. The sensitivity of the chemical efficiency to $\sigma_y(0)$ for three values of the turbulence intensity between 1 and 10^{-2} m^2/sec^2 and for $k = 5\times10^5(pp\text{-}sec)^{-1}$.

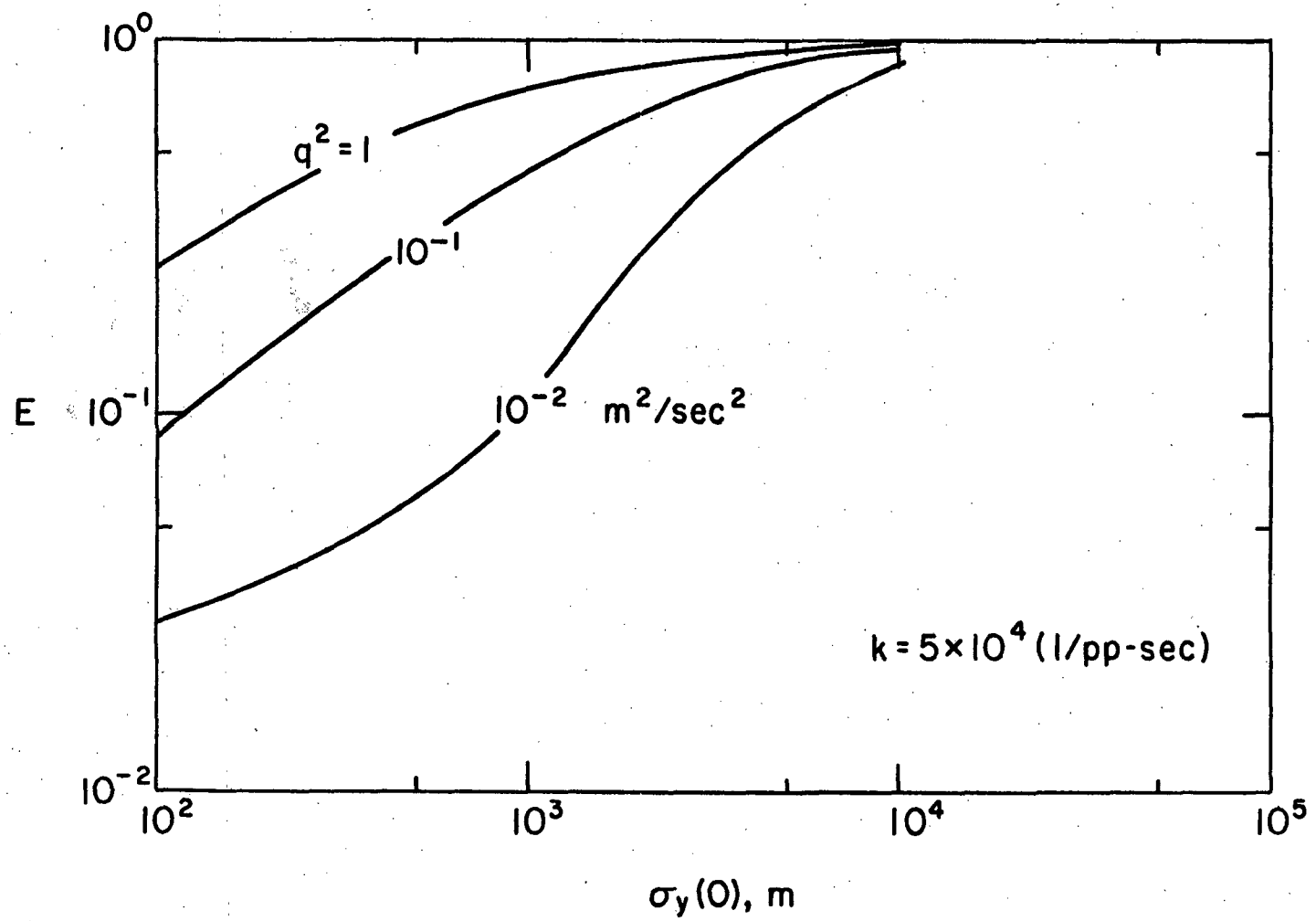

Figure 28. The sensitivity of the chemical efficiency to $\sigma_y(0)$ for three values of the turbulence intensity between 1 and 10^{-2} m^2/sec^2 and for $k = 5 \times 10^4 (pp\text{-}sec)^{-1}$.

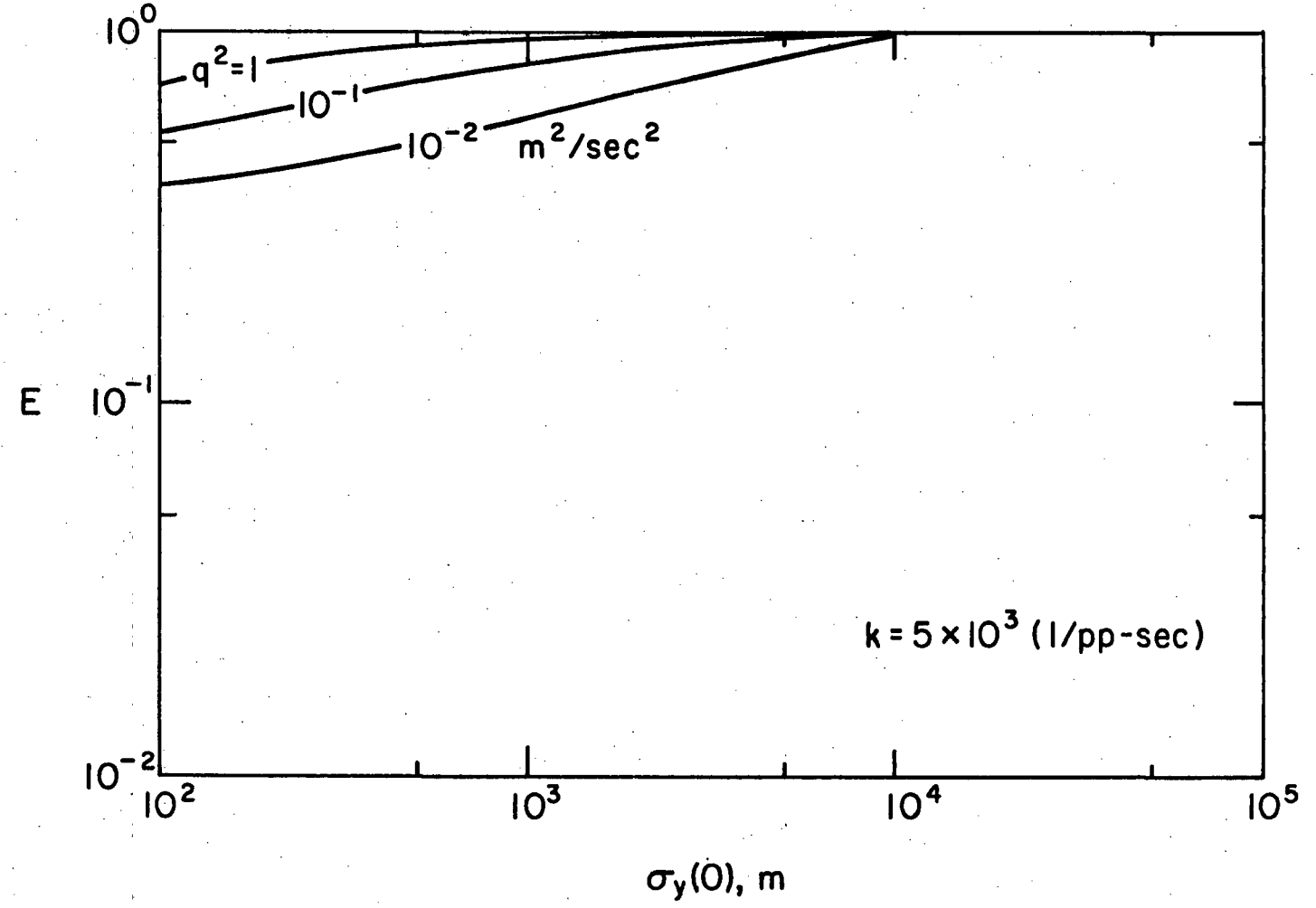

Figure 29. The sensitivity of the chemical efficiency to $\sigma_y(0)$ for three values of the turbulence intensity between 1 and 10^{-2} m^2/sec^2 and for $k = 5 \times 10^3 (pp\text{-}sec)^{-1}$.

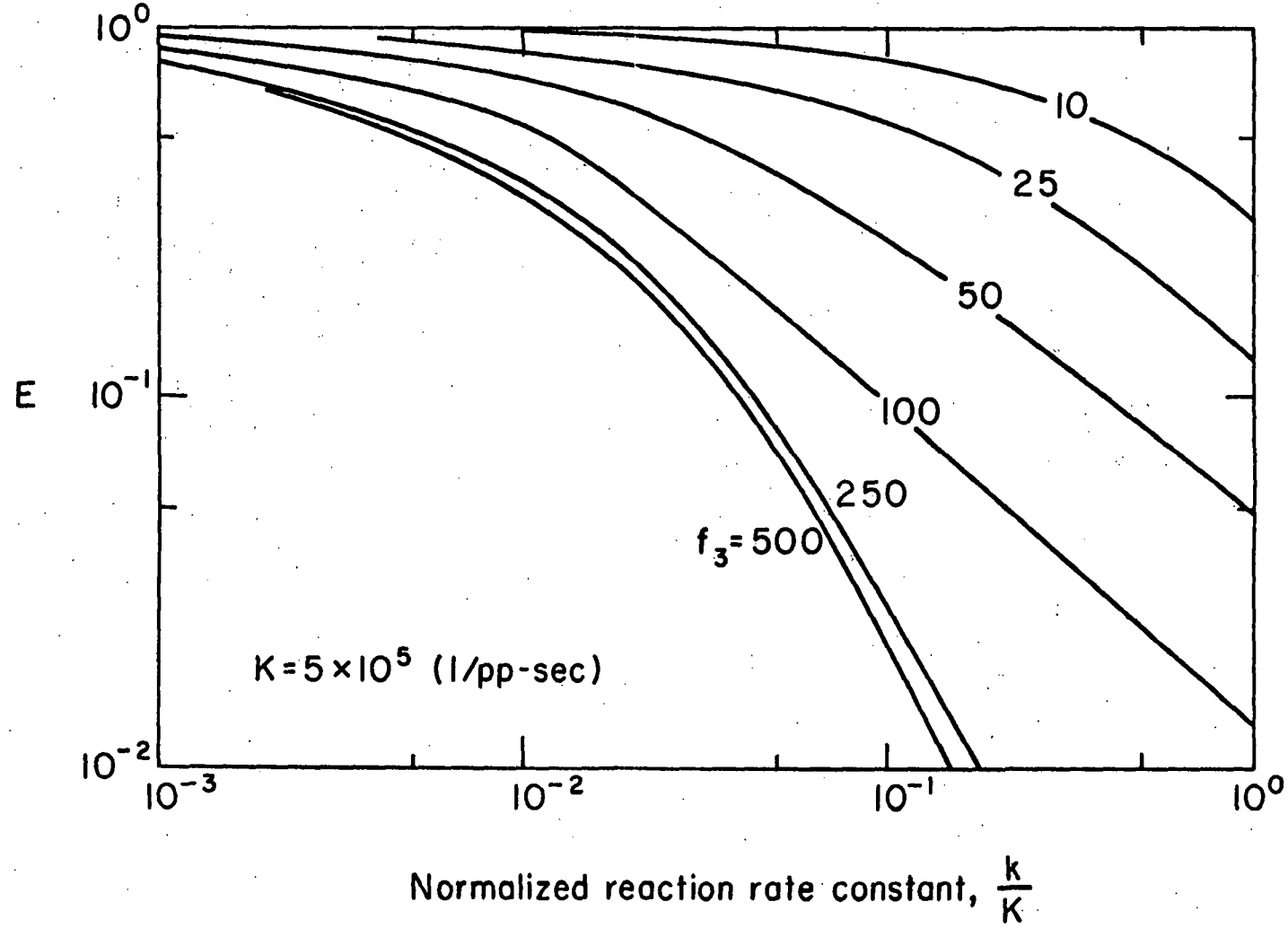

Figure 30. The sensitivity of the chemical efficiency to the reaction rate constant for several values of f_3 where f_3 is a function of Ri , Λ_T and $\sigma_y(0)$.

TABLE 7

ILLUSTRATION OF SENSITIVITY OF E TO INDEPENDENT VARIABLES (BASE VALUE OF E = 10%)			
Independent Variable	Direction of Order of Magnitude Change	Value of Variable	E(%)
q^2	increase	$10^{-1}(m^2/sec^2)$	45
	decrease	$10^{-3}(m^2/sec^2)$	2
σ_y	increase	$10^4(m)$	40
	decrease	$10^2(m)$	3
k	increase	$5\times10^5(1/pp\text{-}sec)$	2
	decrease	$5\times10^3(1/pp\text{-}sec)$	60

Table 7 shows that a tenfold change in any one of the independent variables can result in a five-to sixfold change in the chemical efficiency. It can be demonstrated using Eq. (37) that this variation in E is equivalent to $\overline{E}$ values of between 0.5 and 0.8 when the duration of the wake phase is one half of the plume residence time in the stratosphere. In other words, present estimates of the impact of the SST on the O_3 inventory must be reduced by 20% to 50% - a rather wide variation to say the least - for the conditions chosen. More accurate predictions will require considerably better than order of magnitude estimates of the independent variables. These results, as was noted above, are for purely hypothetical conditions. The reader may choose any combination of variables which he considers to be appropriate for the lower stratosphere and develop his own sensitivity table using the results given in Fig. 25.

We showed earlier that E is less than unity because of the combined effects of diffusion and mixedness limitations. We now examine each of these limitations separately. Figure 31 shows the diffusion limitation, L_D . Recall from the definition of L_D (Eq. (34)), that as L_D approaches unity the reaction stops because the ambient O_3 cannot be diffused rapidly enough into the plume. Conversely, when L_D approaches 0 , turbulent diffusion supplies all the O_3 needed by the reaction. It is clear, in Fig. 31, that the diffusion limitation is most pronounced for very stable turbulence fields, very compact plumes and very fast chemical reactions. The diffusion limitation is diminished as q^2 increases, or σ_y increases, or k decreases.

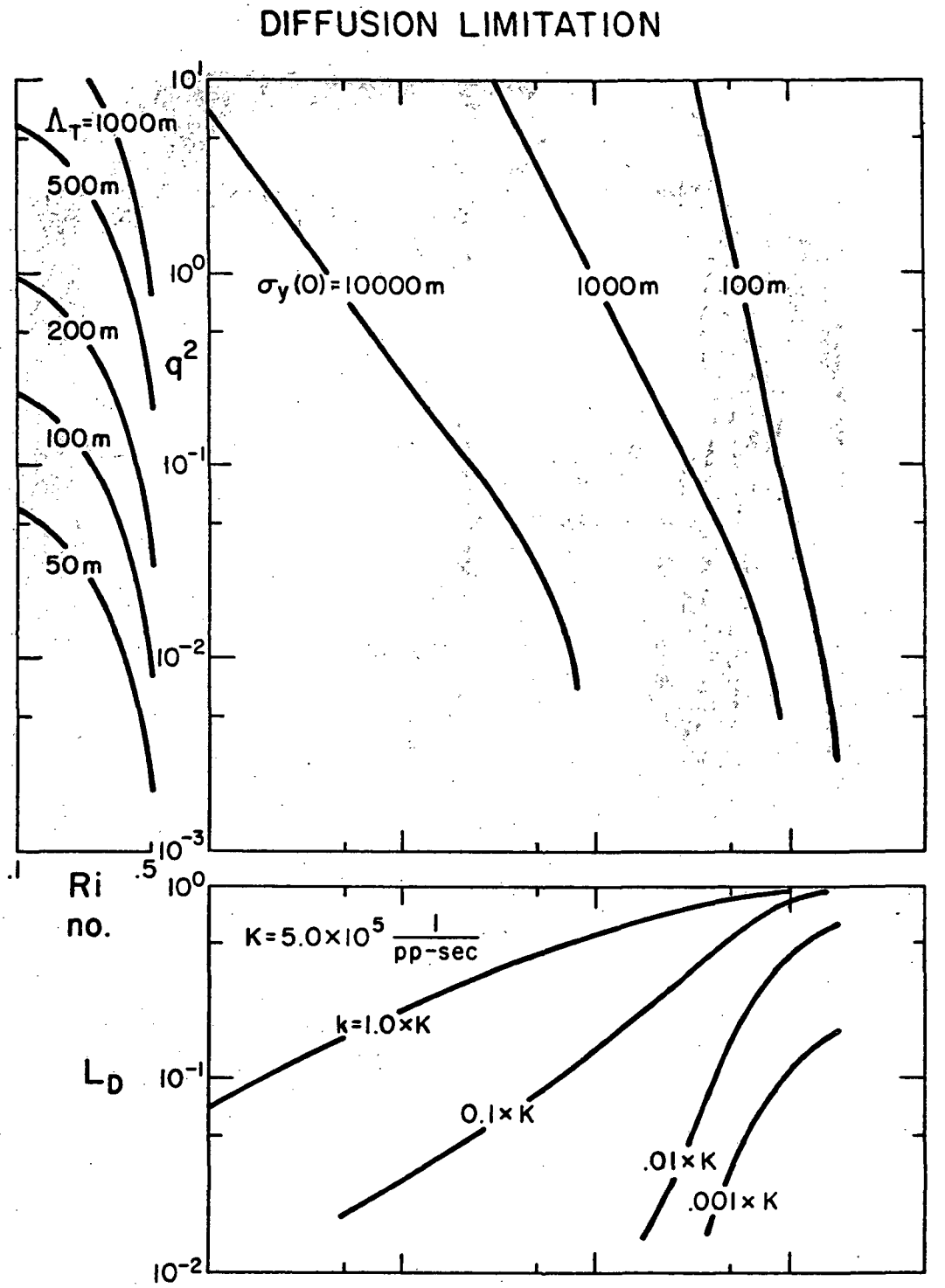

Figure 31. The dependence of the diffusion limitation on the turbulence field, source strength, and reaction rate constant. The diffusion limitation is one component of the efficiency deficit.

Figure 32 shows the effect of k and q^2 on L_D and clearly illustrates the switch from a diffusion limited reaction for large k to a reaction rate-limited condition for small k.

Figure 33 shows the other deficit to E, the mixedness limitation, L_M. In this figure, the iso-k curves have a local maximum. This peaking phenomenon is not completely understood at the present time. However, the important point to glean from Fig. 33 is that L_M is never more than 0.25 for any combination of the independent variables. This suggests that conventional mean value chemistry would, at most, overpredict the depletion rates for O_3 by 25% by neglecting $\overline{C'_\alpha C'_\beta}$.

Figure 34 shows the sensitivity of L_M to k for five levels of q^2. There appears to be no consistent trends other than that L_M is a maximum when the reaction is neither diffusion rate nor reaction rate limited and L_M approaches 0 for both limiting conditions. A careful comparison of Figs. 32 and 34 shows that L_D is always greater than L_M and, therefore, turbulent diffusion is the dominant influence on the O_3 depletion rate.

We conclude this section with three figures showing E, L_D and L_M contours in the q^2-σ_y plane. Similar figures were previously presented in ref. 2 but the data obtained during the present study permitted an extension of the curves to a larger domain and resulted in minor revisions in the original domain. For each of these figures, $k = 5\times10^5$(1/pp-sec).

Figure 35 shows E contours as a function of q^2 and σ_y and again demonstrates the low efficiencies associated with low turbulence intensity and compact plumes. For the most part E varies more rapidly with σ_y than with q^2.

Figures 36 and 37 show the corresponding L_D and L_M contours respectively. These figures clearly pinpoint the regions of maximum diffusion and mixedness limitations which were described earlier.

CONCLUSIONS

In conclusion, we have demonstrated the sensitivity of the coupled chemistry/diffusion model to a wide range of variation of the model's independent variables. We have shown that the efficiency with which the NO_x catalytic cycle destroys ambient O_3 is extremely sensitive to the amount of NO emitted and to the relative rates of turbulent diffusion and chemical reactions. For representative conditions in the stratosphere, the chemical efficiency is roughly 10%. However, a tenfold change in either q^2, k or σ_y can produce a factor of five change in the efficiency. If the duration of Phase III is a significant fraction of the total residence time of the plume, then these efficiency variations can alter O_3 depletion rates by more than a factor of two.

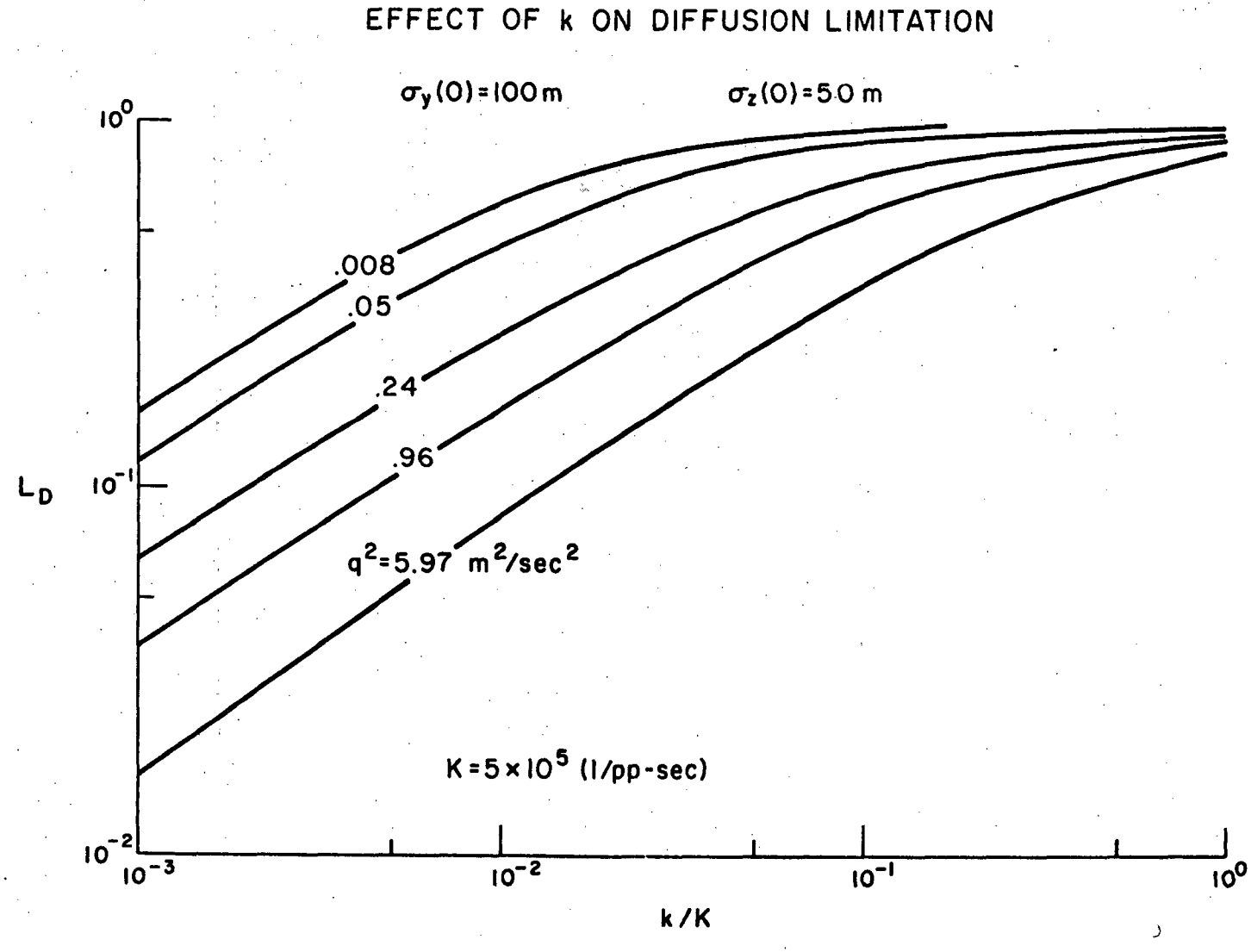

Figure 32. The sensitivity of the diffusion limitation to the reaction rate constant for five values of turbulence intensity between 0.008 and 6.0 m^2/sec^2.

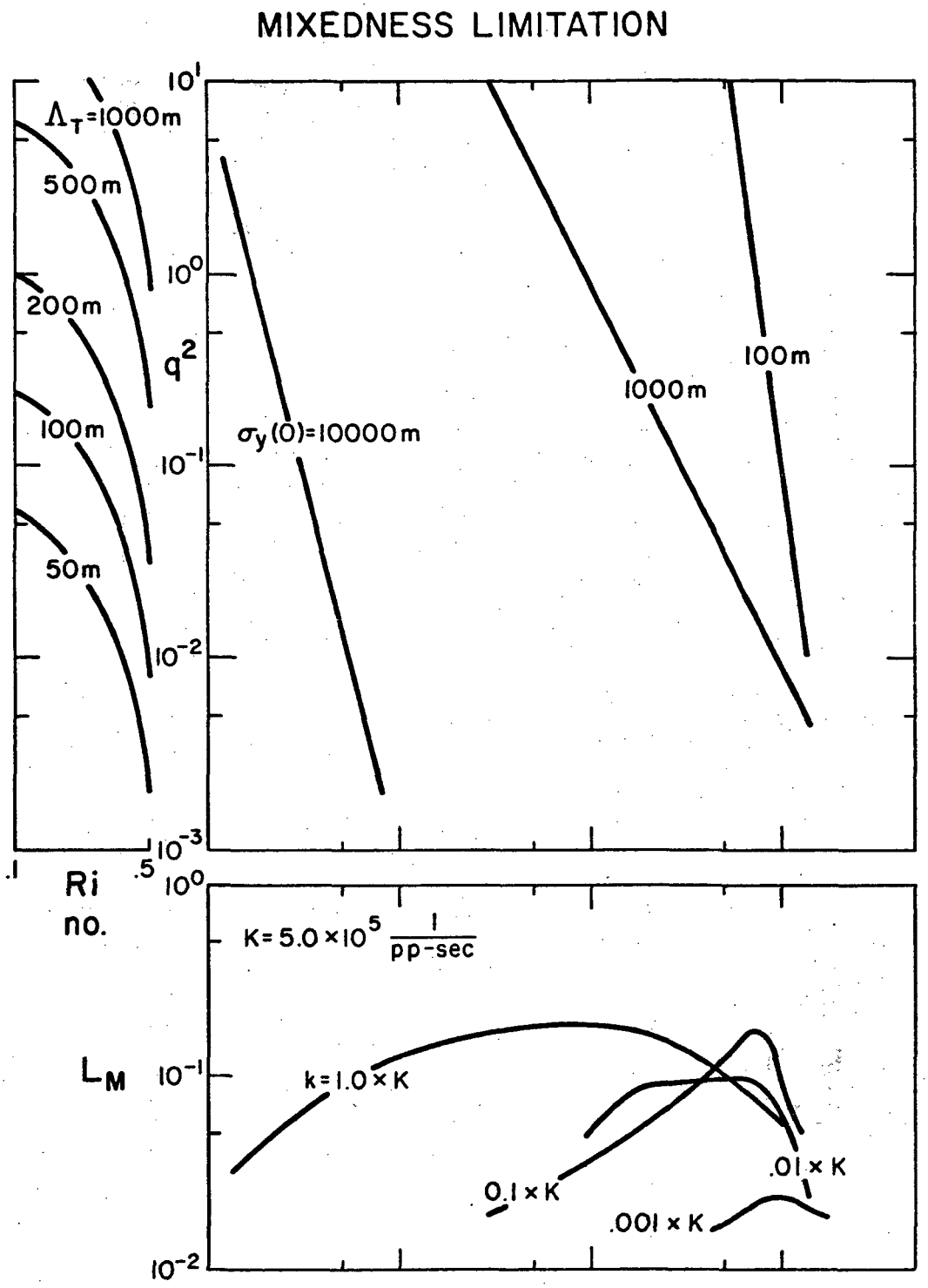

Figure 33. The dependence of the mixedness limitation on the turbulence field, source strength, and reaction rate constant. The mixedness limitation is one component of the efficiency deficit.

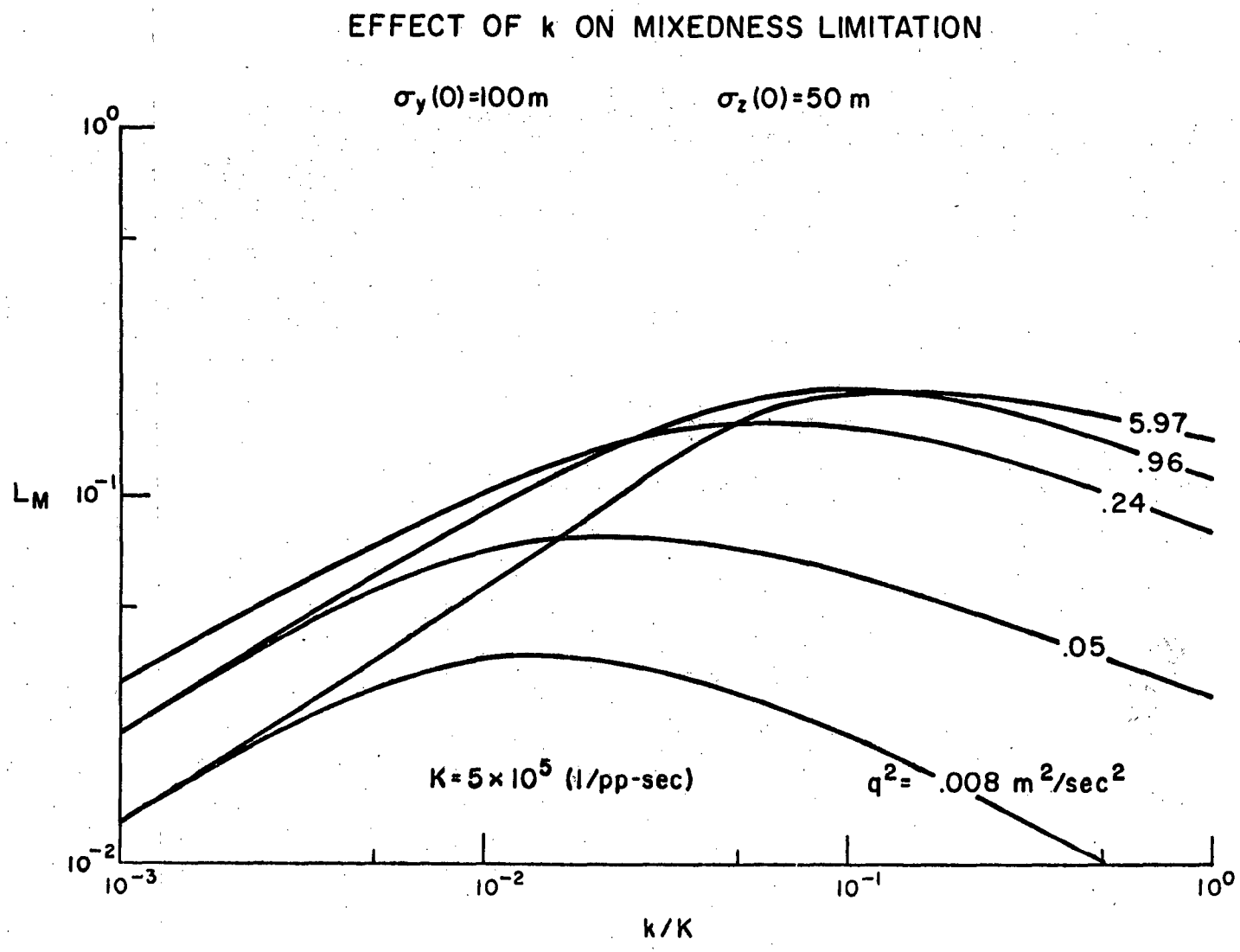

Figure 34. The sensitivity of the mixedness limitation to the reaction rate constant for five values of turbulence intensity between 0.008 and 6.0 m^2/sec^2.

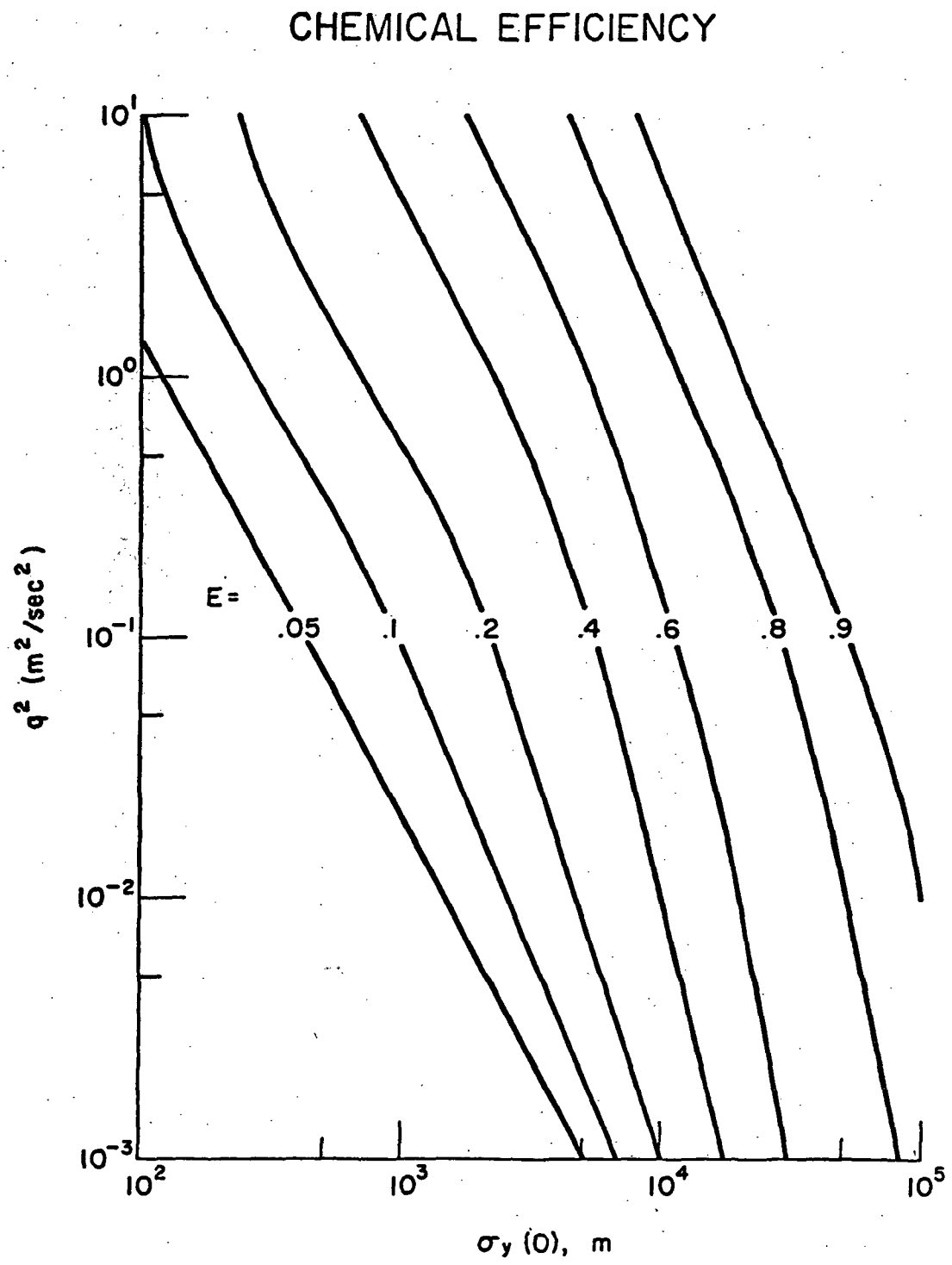

Figure 35. Chemical efficiency contours as a function of q^2 and $\sigma_y(0)$ for $k = 5\times10^5$(pp-sec)$^{-1}$.

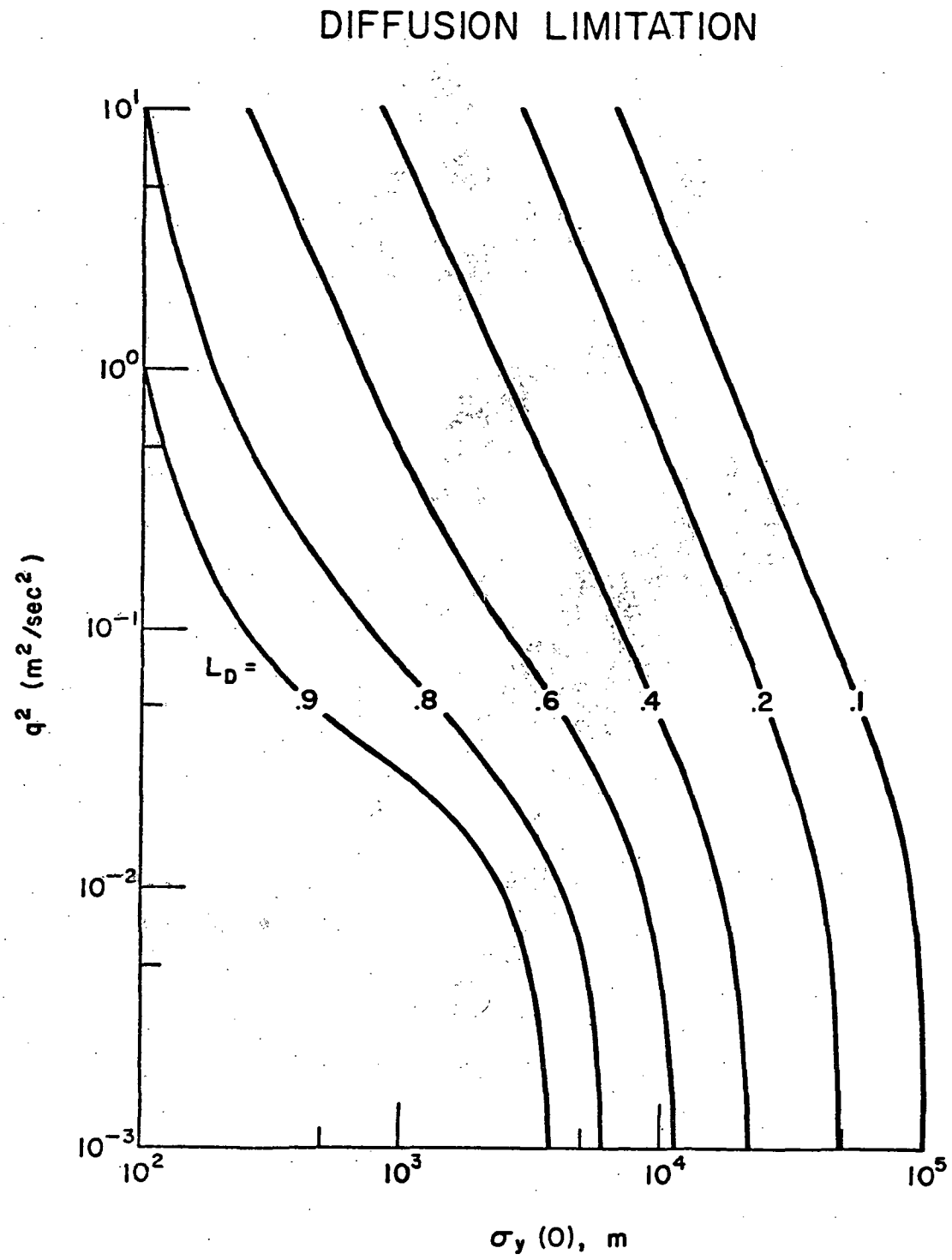

Figure 36. Diffusion limitation contours as a function of q^2 and $\sigma_y(0)$ for $k = 5 \times 10^5 (pp\text{-}sec)^{-1}$.

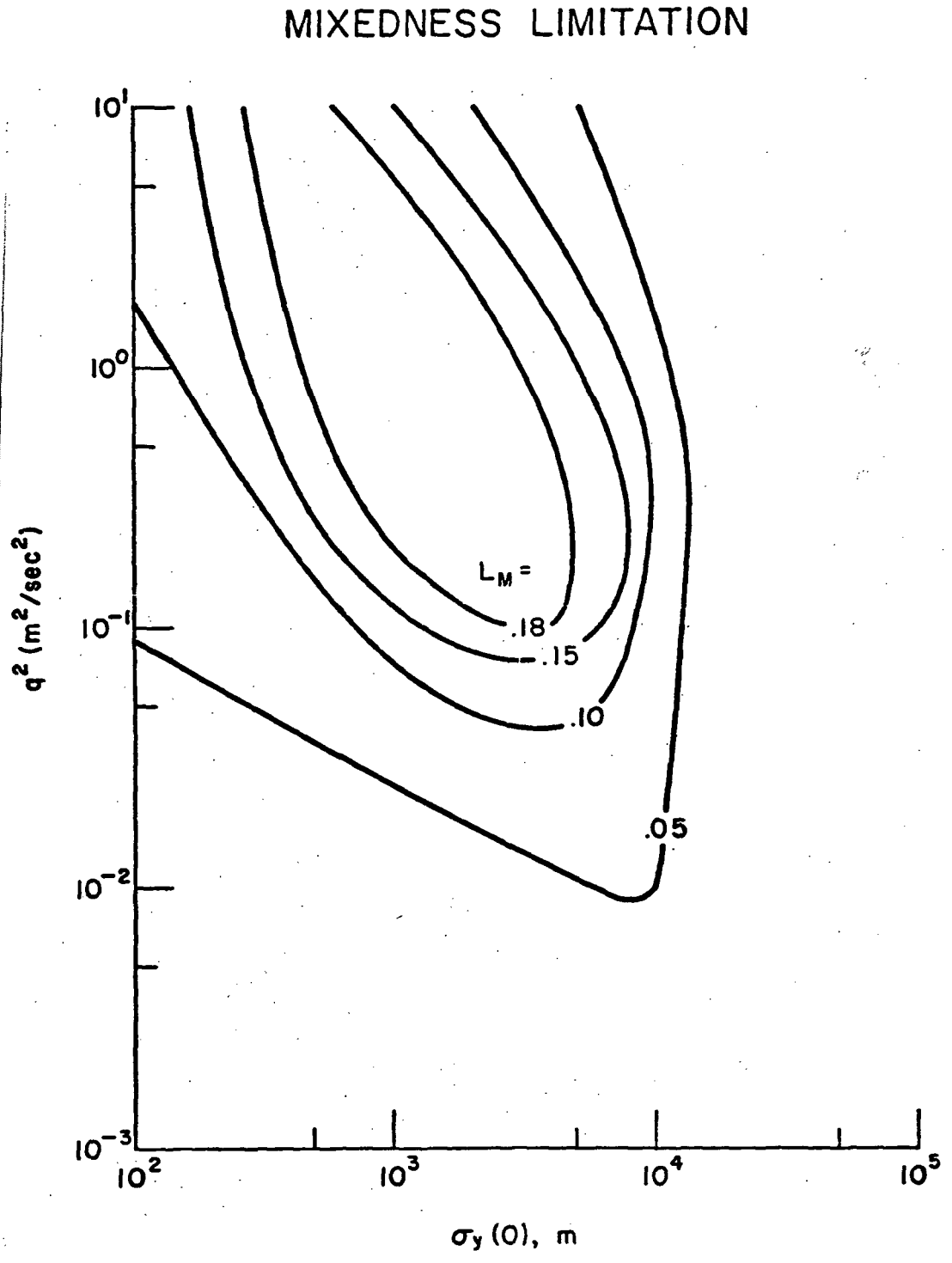

Figure 37. Mixedness limitation contours as a function of q^2 and $\sigma_y(0)$ for $k = 5 \times 10^5 (\text{pp-sec})^{-1}$.

These results point toward those variables which must be accurately defined in order to reasonably estimate the impact of SST fleet operations on the O_3 inventory. In particular, the need for accurate turbulence measurements in the stratosphere is apparent. In addition, better estimates of the residence time of the plume in the stratosphere which take into account the aircraft flight path (i.e. latitude, longitude and altitude of plume injection) are essential.

Finally, these results demonstrate the power of the invariant coupled model. By retaining the second-order correlations in the controlling equations, we have been able to keep track of the separate effects of diffusion, mixedness, and chemistry. We have shown that conventional mean-value chemistry can overpredict the O_3 depletion rate by at most 25% by neglecting the mixedness term $\overline{c'_\alpha c'_\beta}$. This inaccuracy may be acceptable and mixedness may be neglected but only second-order closure techniques can define the magnitude of the error. Even more importantly, we have shown that low turbulent diffusion rates are a dominant factor causing low efficiency. And, therefore, the conventional assumption that the reactants are uniformly mixed at all times is grossly inaccurate and will significantly overpredict the magnitude of O_3 depletion due to the SST.

REFERENCES

1. Hilst, Glenn R., et al.: The Development and Preliminary Application of an Invariant Coupled Diffusion and Chemistry Model. NASA CR-2295, May 1973.

2. Hilst, Glenn R., et al.: Some analyses of the Chemistry and Diffusion of SST Exhaust Materials During Phase III of the Wake Period. NASA CR-132323, July 1973.